PHASE- AND AMPLITUDE-COUPLING ARE TIED BY AN INTRINSIC SPATIAL ORGANIZATION BUT SHOW DIVERGENT STIMULUS-RELATED CHANGES

BY

PARHAM MOSTAME

THESIS

Submitted in partial fulfillment of the requirements
for the degree of Master of Science in Psychology
in the Graduate College of the
University of Illinois Urbana-Champaign, 2021

Urbana, Illinois

Master's Committee:

Professor Sepideh Sadaghiani, Chair
Professor Gabriele Gratton

ABSTRACT

Functional connectivity (FC), thought to provide a window into neural communication, has become a core focus in the study of brain function and cognition. However, there is no consensus on how to conceptualize large-scale FC in electrophysiology. Phase coupling (*PhC*), defined as coupling between the phases of two signals, reflects the synchronization of rhythmic oscillation cycles. Conversely, amplitude coupling (AmpC), defined as coupling between the envelopes of two signals, reflects correlation of activation amplitude. Despite quantifying different electrophysiological properties, the relationship between PhC and AmpC remains largely unknown. We assessed spatial and temporal correspondence between PhC and AmpC over 5 canonical frequency bands during a cue-based motor task using electrocorticography (ECoG) in 18 patients (8 females) undergoing presurgical monitoring. Significant correspondence between the spatial pattern of PhC and AmpC was detected during stimulus processing across all subjects and frequency bands ($R \approx 0.50$ for theta, decreasing with increasing frequency). The cross-measure spatial correlation vanished almost entirely when accounting for the portion of FC equally present during pre- and post-stimulus intervals, suggesting that the spatial correlations reflect intrinsic FC independent of stimulus processing. Stimulus-related processing modulated both PhC and AmpC, however in a spatially independent manner. Examining the linear temporal correlation, we found no evidence for linear dependence between PhC and AmpC. Supporting the robustness of our findings, results extended to a verb generation task in a second ECoG dataset of 6 subjects. We conclude that PhC and AmpC reflect intrinsic FC similarly across space, but exhibit divergent stimulus-related FC changes over space and time.

ACKNOWLEDGMENTS

I am greatly thankful to Dr. Graham Huesmann for discussions of ECoG data quality, and Dr. Kai Miller and colleagues for generously sharing their data. I also want to thank my co-advisor, Dr. Abbas Babajani-Feremi, for educating and preparing me for my academic career with his irreplaceable lessons throughout these years.

Finally, I am very thankful to my supervisor, Dr. Sepideh Sadaghiani, for her priceless mentorship. Without her unique leadership, thoughts, viewpoints, and knowledge this work would have not existed today.

Dedicated to my family for their consistent support throughout my life and my academic career.

In the hope that this will, at least partly, compensate for their invaluable favors to me.

TABLE OF CONTENTS

CHAPTER 1: INTRODUCTION[1]

Communication across distant neural populations is a principal mechanism of brain function and cognition (Varela et al., 2001; Singer, 2013). Functional connectivity (FC), defined as temporal dependence among measures of remote neurophysiological processes (Friston, 1994), is thought to (at least partly) reflect such mechanisms based on the association that has been demonstrated between FC changes and behavior (Uhlhaas et al., 2009; Fell and Axmacher, 2011). Neurophysiological (MEG, EEG, and intracranial EEG) studies use fundamentally different approaches to measuring FC (Fig. 1), one based on temporal dependence of oscillation phase (phase coupling, or PhC) and the other of oscillation amplitude (amplitude coupling, or AmpC) (for second-order, cross-frequency dependencies beyond the scope of the current study see Ryan T. Canolty et al. 2010; J. M. Palva and Palva 2018). Neurophysiological studies of task-evoked functional connectivity commonly use phase coupling (PhC) (e.g. Gandal et al. 2012; P. J. Uhlhaas and Singer 2012), while amplitude coupling (AmpC) has been traditionally employed in task-free resting state studies (e.g. Brookes et al. 2011; De Pasquale et al. 2010; Hipp et al. 2012). Although PhC and AmpC are conceptualized to constitute two mechanistically different coupling modes (Engel et al., 2013), quantitative comparisons between the two FC modes are largely outstanding. Consequently, there is a missing link between the two bodies of literature that use PhC or AmpC.

PhC is a widely-used approach assessing FC of neurophysiological signals (Varela et al., 2001; Singer, 2013). PhC measures estimate how consistently the phases of two different signals are locked to each other over many repetitions of an experiment or over consecutive oscillation

cycles, in each specific frequency (Nolte et al., 2004). Thus, by definition, PhC detects connectivity across different areas based on synchronizations of the oscillation cycles of rhythmic activity across the respective neuronal populations (Fig. 1).

AmpC has only recently gained prevalence in neurophysiological studies (De Pasquale et al., 2010; Brookes et al., 2011; Hipp et al., 2012). This newfound popularity is largely driven by the similarity of AmpC to measures of FC in functional Magnetic Resonance Imaging (fMRI) literature. Several studies have shown that task-evoked changes in envelope of neurophysiological signals are correlated with Blood Oxygen Level Dependent (BOLD) fluctuations of fMRI (Singh et al., 2002; Brookes et al., 2005; Zumer et al., 2010). On the other hand, FC in fMRI literature is most commonly assessed by estimating temporal correlations of BOLD signals across distant brain areas (Biswal et al., 1995; Greicius et al., 2003; Fox et al., 2005). In a similar vein, AmpC in neurophysiological signals is estimated as the temporal correlation between the envelopes of (band-pass filtered) signal timecourses. By definition, AmpC detects the similarity of (arrhythmic) fluctuations in activation amplitude of two regions, where the amplitude in each region is in turn a function of local synchronization of oscillatory activity within each neuronal population (Fig. 1).

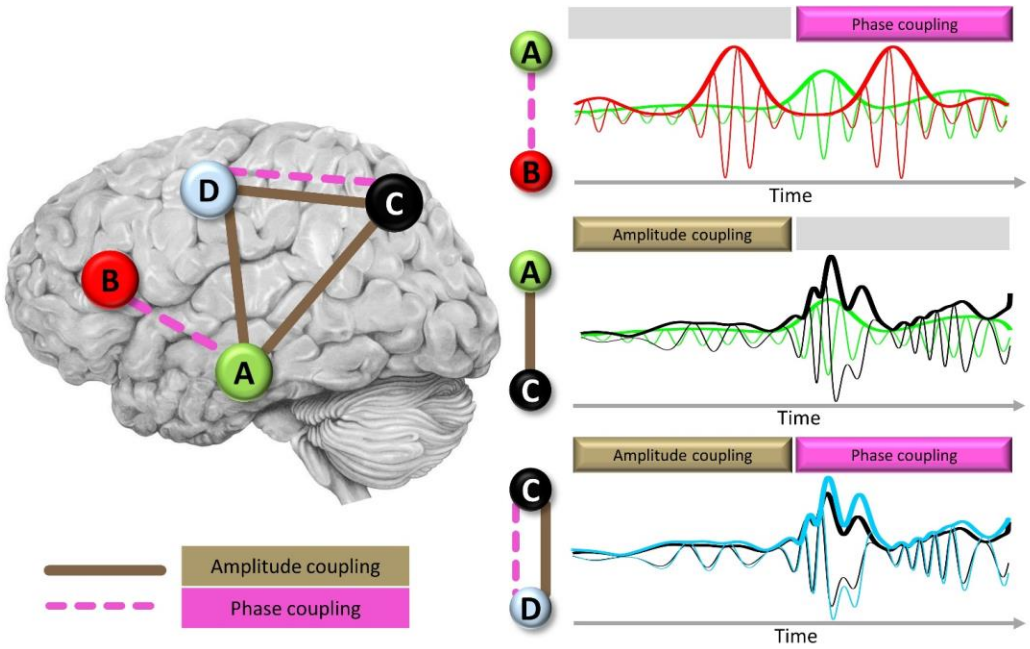

Fig. 1 – Schematic view of PhC and AmpC as two modes of functional connectivity - Left panel: Graph view of FC organization between nodes A, B, C, and D, including links depicting either PhC (dashed pink lines) or AmpC (solid brown lines). Right panel: The narrow lines represent oscillatory neural activity timecourses of the two nodes involved in each connection (connections from top to bottom: A-B, A-C, and C-D). Thick lines show envelopes of the signals obtained using the Hilbert transform. Corresponding colors are used for nodes, oscillatory timecourses, and their envelope. The middle plot shows presence of PhC in the absence of AmpC (A-B) and the middle panel shows presence of AmpC only (A-C). The lower plot shows a case where both PhC and AmpC are present between the two nodes (C-D). Note that AmpC between A-C and C-D also implies AmpC for A-D, which we didn't show in the right panel for simplicity. Reproduced with permission from (Sadaghiani and Wirsich, 2019).

A review study discussing the two disconnected literatures has proposed that PhC and AmpC are two dissociable coupling modes despite relying on a common anatomical connectivity organization (Engel et al., 2013). Beyond such conceptual considerations, experimental comparisons across PhC and AmpC remain rare. At the short distance of few millimeters within a visual brain region, the phase lag at which PhC occurs may be mechanistically linked to AmpC strength (cat/monkey; Womelsdorf et al. 2007). Further, coupling between subcortical spike activity and the phase of cortical LFP is higher for electrode pairs with stronger subcortico-cortical AmpC (ferret; Stitt et al. 2015). Regarding cortico-cortical long-range connectivity, a

rare investigation of both PhC and AmpC in the same task context finds that the two modes connect different sets of brain regions and are linked to different cognitive operations (human scalp EEG; Helfrich et al. 2016). However, the degree to which the two coupling modes correspond or vary in their spatial, temporal, and spectral properties has not been quantified. To our knowledge, no study has directly compared these properties in intracranial data that provide relatively reliable spatial localizability.

Indirect support for spatial similarity of stationary PhC and AmpC emerges from multi-modal studies. Source-projected EEG and MEG whole-brain connectomes are spatially similar to fMRI- and DTI-derived connectomes, irrespective of whether PhC or AmpC is used (Deligianni et al., 2014; Finger et al., 2016; Wirsich et al., 2017). More directly, by estimating PhC and AmpC within the same MEG dataset, high spatial correspondence of their static FC organization has indeed been observed (Hillebrand et al., 2012; Colclough et al., 2016). However, these studies do not relate the temporal evolution of the two coupling modes. More importantly, the studies employ data recorded at the scalp, raising uncertainty concerning connectivity measures due to the fact that source-reconstruction is an inherently ill-posed problem that can lead to spurious long-range dependencies (Schoffelen and Gross, 2009; Palva et al., 2018).

Here, we use intracranial EEG signals in patients undergoing presurgical evaluation for intractable epilepsy to assess spatial and linear temporal correspondence between PhC and AmpC over five canonical frequency bands. We aim to quantify the degree to which the two coupling modes co-engage, or conversely, provide distinct FC “channels” over space and time. The findings will further facilitate comparisons across different neurophysiological studies, and indirectly, with fMRI studies (due to their above-described link to AmpC).

CHAPTER 2: MATERIALS & METHODS

2.1 Data specifications and procedures

We analyzed two publicly available datasets described in detail in Miller (Miller, 2019), freely available at https://searchworks.stanford.edu/view/zk881ps0522. These datasets contained ECoG signals of subjects undergoing presurgical evaluation for epilepsy-related surgery. All patients participated in a purely voluntary manner, after providing informed written consent, under experimental protocols approved by the Institutional Review Board of the University of Washington (#12193). All patient data was anonymized according to IRB protocol, in accordance with HIPAA mandate.

2.1.1 Primary dataset

The primary dataset in this study comprised a finger flex motor task originally investigated in Miller et al. (2007). Among the active tasks available in the public ECoG library, we chose the cue-based basic motor task because it has the largest number of subjects. Subjects -disregarding 3 with missing age information- were on average 30.8 years old (+/- std= 9.6). A 19th patient was excluded because of shorter inter-trial and trial intervals compared to the other subjects. Average number of electrodes per subject was 55.8 (+/- std=10.7) with an inter-electrode distance of 1cm. Patients were instructed to perform a repetitive motor task, specifically synchronous flexion and extension of all fingers, based on a visual word cue indicating the body part that should be moved (an alternative cue instructed tongue movements not analyzed in this study). Movements were self-paced with a rate of ~1-2Hz and on the contralateral side of the cortical grid placement. Each movement interval was 3s long, preceded by a rest interval of the same length (blank screen). To maximize independence between trials, we excluded 0.5s from the two tails of the trial for our analyses, resulting in a [-2.5, 2.5]s interval relative to cue onset. There were between

30 and 75 trials of rest and movement per subject (for more details see Miller et al. 2007). Miller et al. have reported robust task-related power changes in the high frequency or high gamma range (76-100HZ) across all subjects, implying that the subjects have task-appropriate electrode coverage suitable for our study.

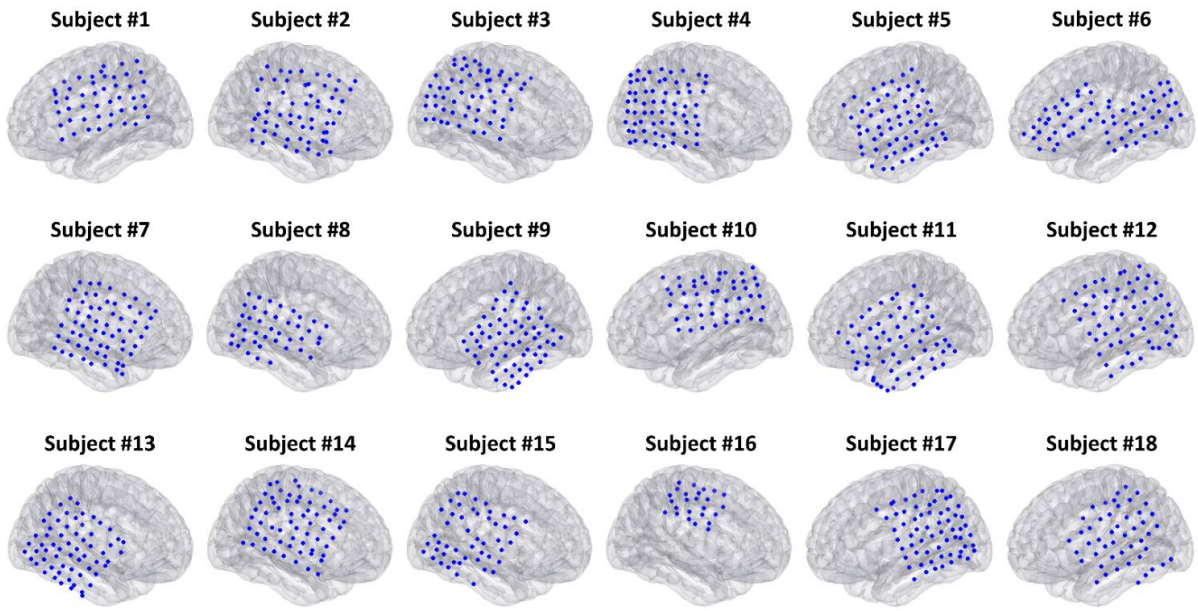

Fig. 2 - Electrode coverage of individual subjects overlaid on a canonical reconstructed cortical surface.

2.1.2 Secondary dataset

We confirmed our results in a second publicly available dataset (cf. Fig. 8). For this purpose, we chose the verb generation task of the same data repository as we aimed at a cognitively demanding task to maximize functional difference to the simple motor task. Among the higher cognitive tasks of the repository, the verb generation task provided the most subjects. From the provided 7 subjects, we excluded one subject who had 10 instead of 40 trials. Four of the 6 subjects were among the 18 subjects of the primary dataset. Further details are provided in a prior investigation using these data (Miller et al., 2011). Subjects -disregarding one with missing

age and sex information- were on average 27.4 years old (+/- std= 10.1; 3 females). On average, subjects had 55.3 (+/- std=8.8) electrodes with an inter-electrode distance of 1cm. Written nouns (approximately 2.5 cm high, and 8–12 cm wide) were presented on a screen positioned approximately 1 m from the patient, at the bedside. Patients were asked to speak a verb that was semantically related to the noun. For example, if the noun read "ball", the patient might say "kick", or if the noun read "bee", the patient might say "fly". Between each 1.6-second noun there was a blank-screen 1.6-second interstimulus interval. To avoid overlap between the trials during data analysis, we defined the trials from -1.5 to 1.5s with respect to stimulus onset.

2.1.3 Preprocessing

Both datasets were sampled at 1KHz. Signals were re-referenced to average reference and filtered with 60 and 120Hz notch filters (2^{nd} order Butterworth) to remove line noise and its harmonics. A 4^{th} order Butterworth high-pass filter with 2Hz cut-off frequency and a 4^{th} order Butterworth low-pass filter with a 120Hz cut-off frequency were used to remove low frequency drifts and high frequency noise, respectively. Data analyses were performed in MATLAB (version R2018a) using custom codes and the FieldTrip toolbox (Oostenveld et al., 2011). The code is available at https://github.com/connectlab/PhC_vs_AmpC_ECoG_Mostame.

2.1.4 Functional connectivity measures

In this study, we used two different measures of functional connectivity; one assessing PhC and the other AmpC. For PhC assessments, we chose the Phase Locking Value (PLV) because PLV I) is a widely used PhC measure, making our observations directly relevant to a large body of literature, II) is the simplest measure of PhC with minimal mathematical assumptions, i.e. directly using the phase difference without additional modifications (Greenblatt et al., 2012; Gordon et al., 2013; Cohen, 2015; Bastos and Schoffelen, 2016), and most importantly III) is

unaffected by fluctuations in power (Lachaux et al., 1999). Note that relative to scalp EEG recordings, FC in subdural ECoG is comparably less affected by volume conduction effects especially for distances ≥~1cm (Rouse et al., 2016; Dubey and Ray, 2019; Rogers et al., 2019). However, if volume conduction contributes even to a small degree to both PhC and AmpC, this could result in spurious spatial and temporal similarity across the two connectivity modes. Suppressing volume conduction effects in one of the two connectivity modes ensures that this confound won't contribute to the cross-mode relationship. Therefore, to show that any spatial similarity between PhC and AmpC is not primarily driven by volume conduction effects, we replicated major findings using two additional widely used measures of PhC that suppress zero-lag connectivity (see supplementary materials section 2 and Fig. 11).

PLV is defined as:

$$PLV(f) = \frac{1}{\mathrm{N}} \left| \sum_{i=1}^{N} e^{j\Delta\varphi_i(f)} \right|$$

Where f is frequency, N is number of trials, and $\Delta\varphi$ is the phase difference between the corresponding frequency components of the two signals. PLV is a measure that estimates how consistent the phase differences of two signals are over many trials. The more consistent the phase difference over trials, the closer the PLV value is to 1; Conversely, the less consistent the phase difference over trials, the closer the PLV value is to 0.

On the other hand, AmpC estimates how well the amplitude of two signals are correlated to each other. To estimate AmpC between two electrodes, we extracted the envelope of the two signals using the Hilbert transform (originally introduced by Gabor 1946), then estimated the Pearson correlation between the two resulting envelopes. Finally, the resulting Pearson correlation values were averaged across trials.

AmpC lies in a range of -1 to 1, while PLV lies between 0 and 1. In other words, PLV is an unsigned measure but AmpC is a signed measure. To compare these two measures, we used the absolute value of the AmpC measure instead of its raw values. This conversion is based on the viewpoint that strong negative amplitude correlations constitute a strong dependency, i.e. connectivity. This step results in a [0 1] scale with comparable functional meaning across PhC and AmpC measures. Specifically, in both measures zero corresponds to lack of functional connectivity, and 1 corresponds to strong functional connectivity.

2.2 Analyses in the static framework

To investigate spatial correspondence between PhC and AmpC we compared the spatial organization of the two FC measures, separately during both pre- and post-stimulus intervals. Additionally, we tested spatial correspondence between the two measures for *task-evoked* FC changes specifically, i.e. post-stimulus FC after accounting for pre-stimulus FC. A generalized flowchart in Fig. 3 depicts analyses of static FC, and details are provided below.

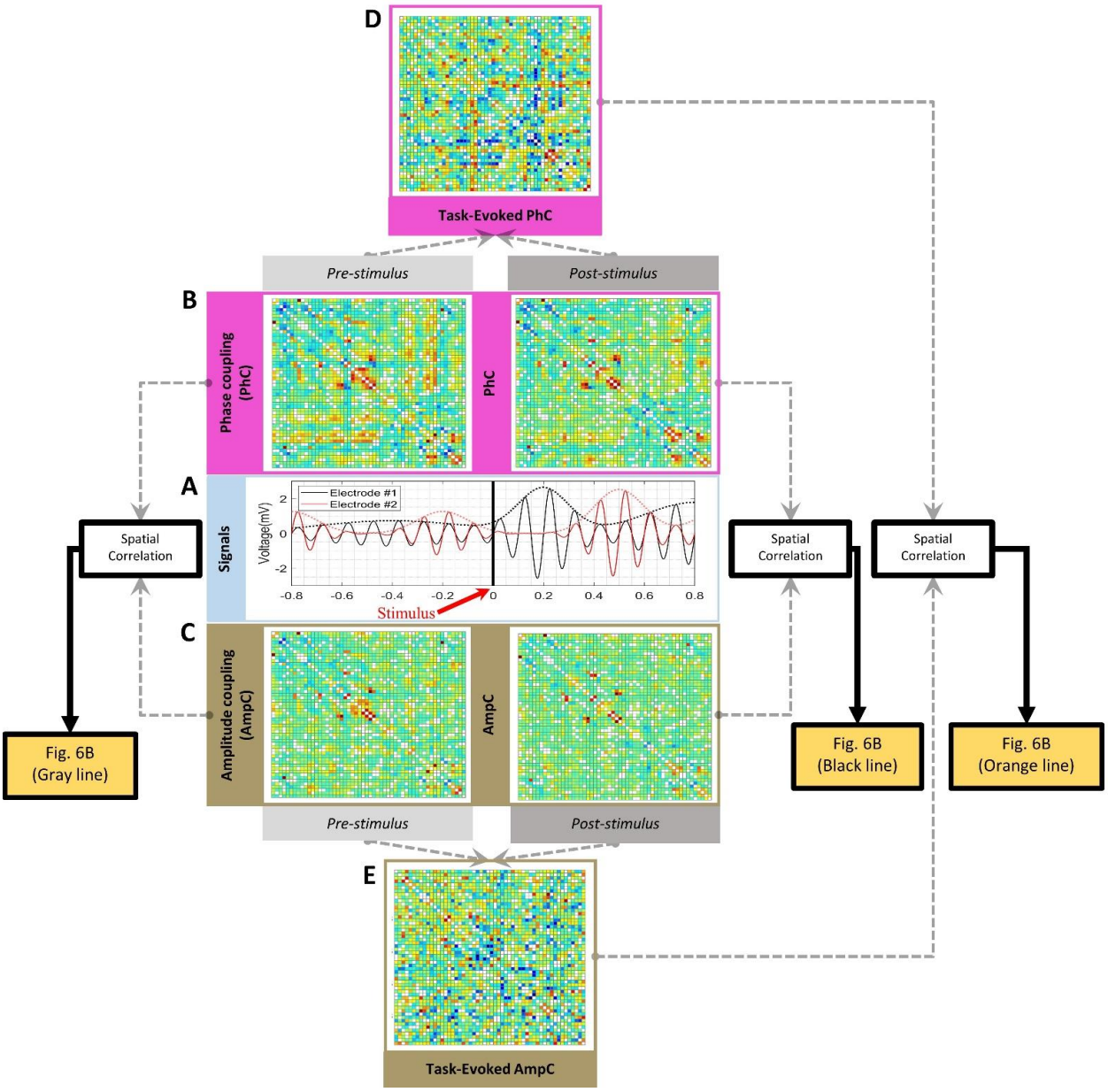

Fig. 3 - Flowchart of analyses in the static framework - This procedure was designed to quantify the spatial correspondence between PhC and AmpC coupling modes. A) Two sample signals with their corresponding envelopes (red and black) during pre- and post-stimulus intervals (left and right to the vertical black line, respectively). B) PhC FC matrices of pre-stimulus (left) and post-stimulus (right) periods. C) Similar matrices for AmpC. D) Task-evoked PhC defined as difference between PhC matrices of the post- and pre-stimulus intervals (connection-wise subtraction). E) The equivalent task-evoked matrix for AmpC. Yellow boxes refer to the respective results figures.

2.2.1 Functional connectivity

For each electrode pair, PLV was calculated as the consistency of the phase lags over trials, where the phase of a given frequency was calculated for the entire 2.5s window (1.5s respectively for the secondary dataset) following the stimulus (post-stimulus time period). Similarly, AmpC was calculated as Pearson correlation of the Hilbert amplitude over all data points within the same time periods for each trial, then averaged over all trials. Additionally, we calculated PhC and AmpC using the same approach for the entire 2.5s window (1.5s for the secondary data, respectively) *preceding* the stimulus (pre-stimulus time period). An equal window length was chosen for the pre-stimulus interval to avoid any biases between pre- and post-stimulus conditions. Finally, to assess the extent to which static FC remains stable or changes due to the task at hand, we subtracted pre-stimulus from post-stimulus FC values for each electrode pair. We refer to the ensuing baseline-corrected FC matrix as task-evoked FC (c.f. Fig. 3D & E).

2.2.2 Impact of distance

Functional connectivity is likely dependent on the distance between the two sites, expected to be stronger for closer electrode pairs than for distant electrode pairs (Kopell et al., 2000; Betzel et al., 2019; Rogers et al., 2019). For results that rely on spatial patterns, we report the relationship across PhC and AmpC before accounting for distance dependencies (Fig. 6A & B), and additionally show findings after regressing out the impact of distance from both measures (Fig. 6C). This regression permits us to quantify the contribution of electrode distance to the spatial relationship between PhC and AmpC. Additionally, it may reduce the impact of any potential volume conductance, as the latter is a function of distance (Rouse et al., 2016; Dubey and Ray, 2019; Rogers et al., 2019).

To assess the dependence of each coupling mode on distance between the two sites, distance between each electrode pair was estimated using MNI locations provided with the data. First, we confirmed that PhC and AmpC are indeed negatively correlated with electrode distance across all subjects and frequency bands, using linear regression (Fig. 4A; PhC significantly more dependent compared to AmpC; $F_{(1.00,\ 17.00)}$=48.084; p=2.41e-6). Next, for each subject and frequency band we removed the impact of distance on both measures as follows (similar to (Hacker et al., 2017)). To this end, we fit cubic spline curves to the mean of the functional connectivity values within each non-overlapping 1cm range of electrode distance. We subtracted the value of the fitted curve from all corresponding functional connectivity values (Fig. 4B). By using this procedure, we removed any possible collinearity between the two measures resulting from their dependence on electrode distance.

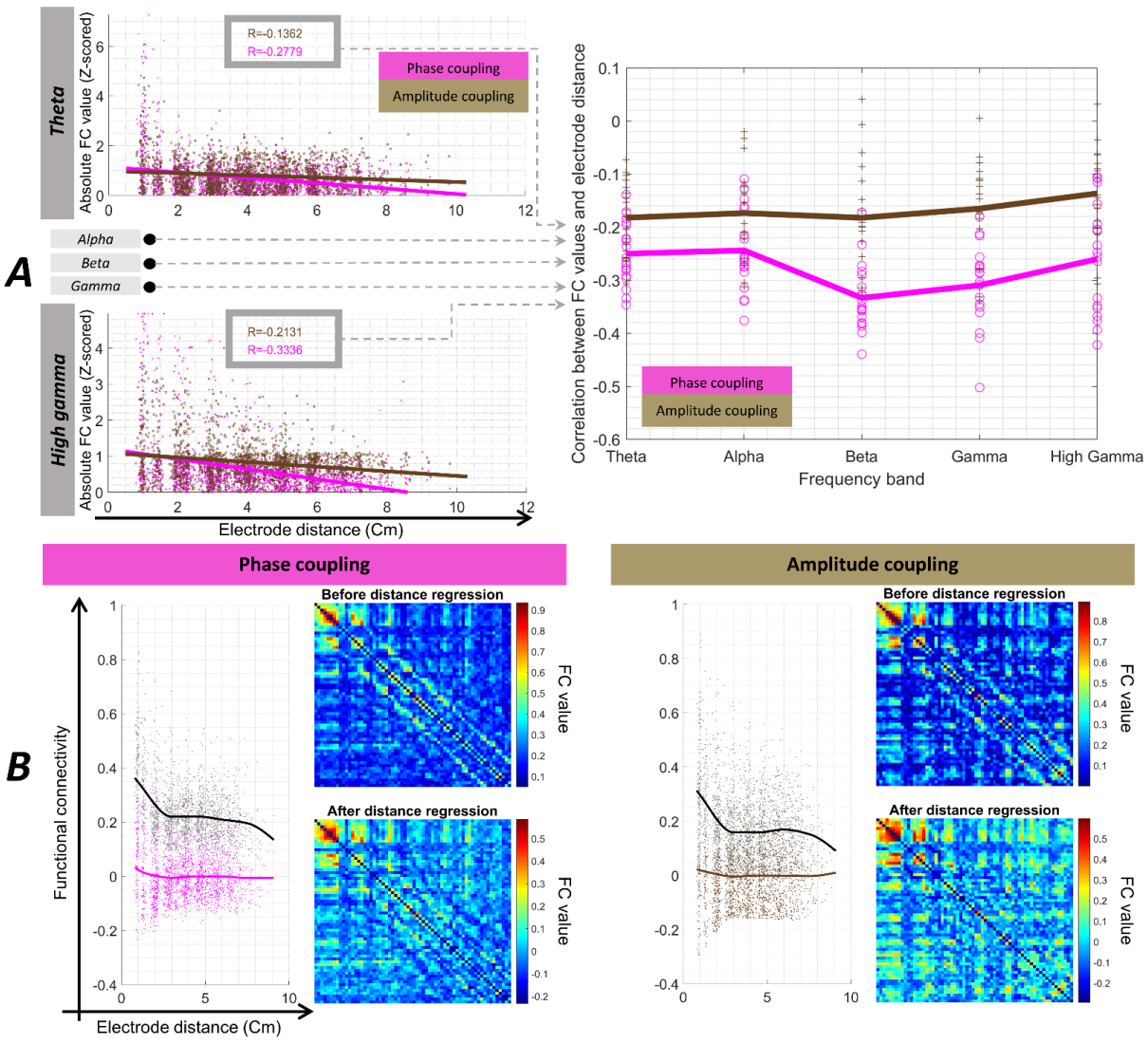

Fig. 4 – Impact of electrode distance - A) using linear regression, the dependency of PhC and AmpC on electrode distance was quantified for all subjects and frequency bands. The left panel show an example for theta and high gamma of an individual subject (each datapoint is one electrode-pair). The right panel shows the FC to distance correlation value for the entire group (one datapoint per subject and frequency). PhC showed significantly higher distance dependency compared to AmpC across all frequency bands (one datapoint per subject and frequency). This implies that PhC has a more localized FC organization and drops off at longer distances, while AmpC is better preserved over long distances. B) Dependency of PhC (left panel) and AmpC (right panel) on electrode distance was regressed out using spline fitting. Data are shown for an individual subject with each datapoint representing one electrode-pair. For PhC and AmpC respectively, the scatterplot to the left shows the FC values before (black) and after (pink for PhC and brown for AmpC) regression. Thick lines with corresponding colors depict averaged FC values as a function of electrode distance. For PhC and AmpC respectively, FC matrices to the right are shown before (top) and after (bottom) regressing out electrode distance. All further analyses were applied to the regressed-out version of FC matrices unless stated otherwise.

2.2.3 Spatial similarity of FC organization across PhC and AmpC

We estimated spatial Pearson correlation between the two static FC matrices of PhC and AmpC. For every frequency band, this correlation was assessed separately for the pre- and post-stimulus intervals. Similarly, we assessed spatial correlation for *task-evoked* FC changes, i.e. for the post-minus pre-stimulus difference matrix (see Fig. 3). Additionally, spatial correlations after accounting for distance dependencies are provided in Fig. 6C. The spatial correlation across PhC and AmpC was tested against the spatial correlation distribution in null model data. Paralleling previous uses of phase-based technique (Prichard and Theiler, 1994; O'Neill et al., 2015; Tewarie et al., 2016), the null model data consisted of 1,000 surrogate datasets generated by randomly permuting the phases of matrices in the 2D Fourier space. Specifically, we transformed each PhC matrix to the 2D Fourier space, randomly permuted its phases -while the magnitude was unchanged- and reconstructed the image using inverse 2D Fourier transform. Note that the phase symmetry over the whole matrix was kept intact so that the reconstructed image does not have imaginary components (Tewarie et al., 2016).

2.3 Analyses in the dynamic framework

To assess dynamics of FC measures, for each electrode pair we normalized the post-stimulus sliding window FC with respect to the 0.5s window of pre-stimulus time varying FC (Sederberg et al., 2003; Hanslmayr et al., 2007; Schölvinck et al., 2013). Then, temporal correlations between the post-stimulus PhC and AmpC dynamics were estimated to investigate linear dependencies between the two coupling modes. This approach permitted answering whether PhC and AmpC have dissociable timecourses. The flowchart of dynamic FC analyses is shown in Fig. 5, and details are provided below.

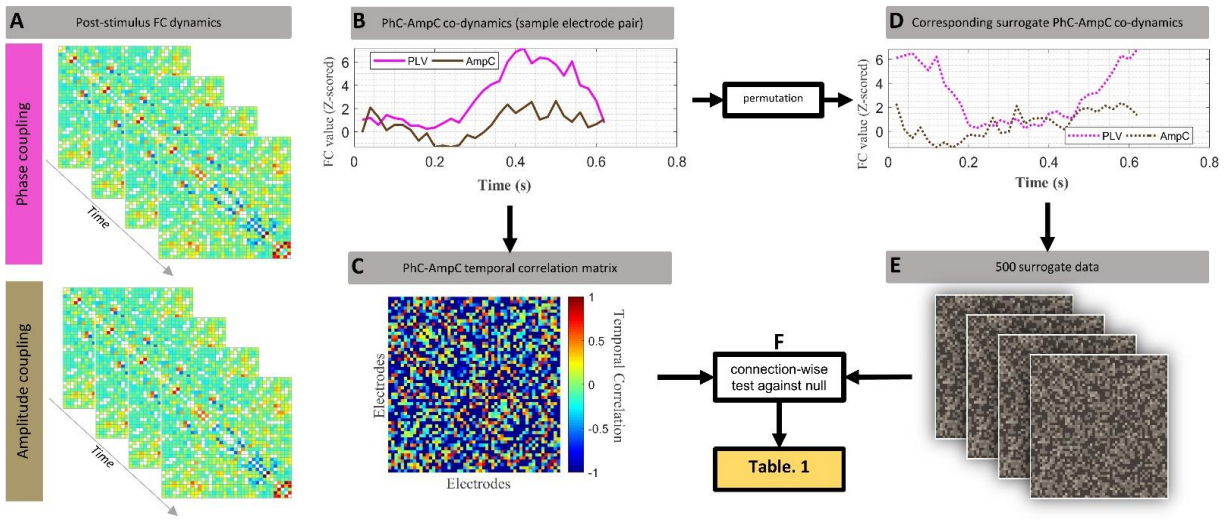

Fig. 5 – Flowchart of analyses in the dynamic framework – This procedure was designed to investigate linear temporal correspondence between PhC and AmpC coupling modes. The pipeline was applied separately for each oscillation frequency. A) The upper panel shows PhC for all electrode pairs calculated within a time window sliding at 20ms steps over the post-stimulus interval and normalized to a 0.5s pre-stimulus interval. This procedure results in one connectivity matrix per time window, where window width is a function of the oscillation frequency. The lower panel shows the equivalent procedure for AmpC. B) Dynamic timecourse of each measure for a sample electrode pair (pink: PhC, brown: AmpC). C) Correlation matrix containing temporal correlation between the two dynamics for each individual electrode pair. D) Surrogate dynamic timecourse of AmpC (dashed brown) and of PhC (dashed pink) generated by randomly shuffling phases of the FC timecourse in Fourier space. E) Set of 500 surrogate matrices of PhC-AmpC temporal correlations which was used to assess significance of PhC-AmpC temporal correlations across electrode pairs. F) Finally, testing against the null distribution from the surrogate data ($q<0.05$ corrected for number of electrode pairs), each electrode pair was labeled as one of the following cases of PhC-AmpC co-dynamics: negatively correlated, uncorrelated (not different from null), and positively correlated. The yellow box refers to the respective results table.

2.3.1 Functional connectivity

We estimated the dynamics of functional connectivity between every electrode pair by using the same PLV and AmpC measures introduced in section 2.1.4, within a sliding time window for the –0.5 to 2.5s time range relative to stimulus onset (-0.5 to 1.5s for secondary data, respectively). The windowed procedure reflects the common approach to task-related connectivity of neurophysiological signals in the literature (Sederberg et al., 2003; Hanslmayr et al., 2007;

Schölvinck et al., 2013). For each time window, we used the multi-taper windowing method (Mitra and Pesaran, 1999) to assess time-frequency analysis with a frequency smoothing parameter equal to 0.15 of the center frequency. We shifted the window by 20ms steps. The length of the window was dependent on the corresponding frequency, and for theta (5-7Hz), alpha (8-13Hz), beta (14-30Hz), gamma (31-60Hz), and high frequency activity or high gamma (61-110Hz) bands was equal to 4, 6, 10, 20, 20 cycles of the corresponding center frequency. FC was averaged over the frequencies within the given canonical frequency band, resulting in a single time course of the functional connectivity dynamics for each electrode pair, measure, and frequency band. For AmpC dynamics, we used the absolute value of the envelope correlations as described above. Subsequently, for each coupling measure we z-scored the dynamic post-stimulus time course of each electrode pair with respect to the 0.5s pre-stimulus baseline window to detect task-evoked FC changes.

2.3.2 Spatial characterization of task-involvement

To address the degree to which task-related changes in one coupling measure are accompanied by changes in the other measure within the same region pairs, we determined which connections (electrode pairs) showed stimulus-related change compared to pre-stimulus baseline in each measure. To this end, we imposed a Monte-Carlo permutation test (R=500) on the pre- and post-stimulus intervals (500ms each in both datasets) for each electrode pair and each measure to determine whether there was a significant change in FC dynamics due to the stimulus (see illustration in the inset of Fig. 7; at a conservative threshold of $q < 0.01$ Benjamini-Hochberg FDR corrected for all electrode pairs of each subject). The interval of 500ms is long enough to provide a sufficient number of time points for the statistical test, and at the same time short enough to ensure that dynamic FC changes within each interval do not cancel each other out. We

compared the percentage of electrode pairs showing significant change in response to the stimulus in either or both FC modes (Fig. 7). For subsequent analyses of temporal dynamics, we retained electrode pairs showing a significant increase or decrease in at least one of the two measures.

2.3.3 Temporal correlations of PhC and AmpC timecourses

Once timecourses of both FC measures were normalized with respect to pre-stimulus baseline, we estimated Pearson correlation values between the 2.5s (1.5s for secondary data) post-stimulus time course of the two measures for all electrode pairs, resulting in a $K \times K$ matrix where K is the number of electrodes (Fig. 5C). To assess significance of these temporal correlations, we generated a null distribution of correlations from 500 surrogate datasets. To generate each surrogate dataset, we randomly permuted the phases of the two measures across frequencies in the frequency domain for all electrode pairs. Next, we estimated the Pearson correlation between the two permuted timecourses for each electrode pair. We extracted the percentage of electrode pairs with positively and negatively correlated dynamics of PhC and AmpC by comparing original correlation values with the null distribution ($q < 0.05$, Benjamini-Hochberg FDR-corrected for number of electrode pairs, Table. 1).

CHAPTER 3: RESULTS

In this study, we measured PhC (specifically PLV) and AmpC in ECoG data to assess both static and dynamic FC during a cue-based motor task. For each canonical frequency band, we generated static FC matrices for PhC and AmpC and assessed their spatial correlation. In terms of time-varying dynamics, we further quantified temporal correlations of PhC and AmpC timecourses over the course of stimulus processing. The correlations in the static framework address to what extent PhC and AmpC covary over space, while the correlations in the dynamic framework assess whether their timecourses are linearly dissociable. Additionally, we demonstrate independence of our findings from particular task demands using a second ECoG dataset during a verb generation task.

3.1 Static framework

In this section, we will assess whether the spatial organization of FC is similar across PhC and AmpC modes. As shown in Fig. 3, we estimated FC matrices of PhC and AmpC as consistency of phase lags over epochs or as Pearson correlations of the Hilbert amplitude, respectively, in the 2.5s post-stimulus and the 2.5s pre-stimulus intervals. Then, we assessed task-evoked (i.e. baseline-adjusted) FC organization of both coupling modes.

3.1.1 Spatial similarity of static FC organization across PhC and AmpC

We extracted post-stimulus PhC and AmpC static FC matrices of all subjects over 5 canonical frequency bands (Fig. 6). Theta band connectivity matrices of the two measures are shown individually for 5 of the subjects in Fig. 6A, demonstrating similarity in the spatial organization of PhC and AmpC. For visualization purposes only, we further used a graph measure called “degree” to localize FC “hotspots” in brain space for PhC and AmpC (the right and left columns in Fig. 6A, respectively). Weighted degree of an electrode is defined as the average connectivity

strength for each electrode to all other electrodes (Rubinov and Sporns, 2010). FC degree maps show which areas of the brain are the high-degree hubs of the FC organization. FC hubs were located consistently across PhC and AmpC, but also highlighted some slight divergences between measures.

To quantitatively compare PhC and AmpC static FC organization, we calculated spatial correlation between the two FC matrices of the post-stimulus interval (i.e. the matrices shown in Fig. 6A) in each frequency band. Fig. 6B shows the Pearson correlation values for all subjects and frequency bands (black line and dots). We found that the static FC organization in PhC and AmpC is highly correlated over space, especially in lower frequency bands (R=0.50 to 0.31 for theta to high gamma frequency bands, respectively). We tested the significance of the spatial cross-measure correlation against a null distribution of 1,000 surrogate datasets generated by randomly permuting the phases of matrices in the 2D Fourier space (dot clouds in Fig. 6B). The spatial correlation between PhC and AmpC was significant for all individual subjects and frequency bands, except for 3 out of 90 cases ($q < 0.005$ corrected for 90 (5 frequencies × 18 subjects) multiple comparisons by Benjamini-Hochberg method). Further, a one-way ANOVA showed a significant effect of frequency on the cross-measure correlation ($F_{(2.04, 34.76)} = 17.58$, p = 4.65e-6), confirming the gradual decrease of the cross-measure relationship from theta to high gamma.

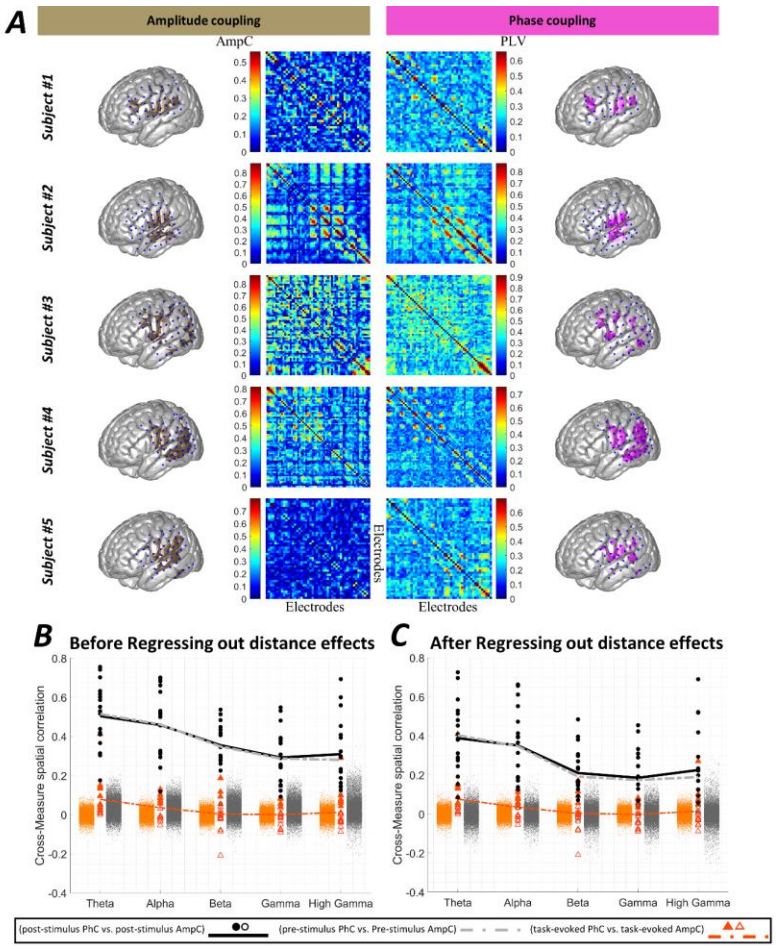

Fig. 6 - Spatial correspondence between PhC and AmpC before (A & B) and after (C) regressing our distance dependencies - A) The matrices show static AmpC (left panel) and PhC (right panel) of 5 subjects (rows) for the theta band. For visualization purposes, corresponding FC degree maps rendered on a canonical reconstructed cortical surface in MNI space are located on the outer side of each panel (see main text for details). B) The black line depicts spatial correlation values between static PhC and AmpC of the post-stimulus period (mean over subjects). Equivalent spatial correlations are shown for the pre-stimulus interval as dashed gray line (mean over subjects). The orange line shows correlation values between task-evoked static PhC and AmpC, i.e. post-stimulus FC after subtraction of pre-stimulus FC. Circles/triangles show R values of all single subjects (Filled=significantly different from null distribution; Unfilled=non-significant). Scattered orange/gray dot clouds show correlation values of the null models for the post-stimulus and task-evoked cross-measure correlations, respectively. Spatial organization in the two FC modes was significantly correlated in all bands and for all individual subjects except for 3 cases (out of a total of 90 cases of subject and frequency bands), and this spatial correspondence was largely accounted for by spatial organization already present prior to stimulus onset. C) Corresponding values of the spatial correlations after regressing out electrode distance. Same major findings remain valid with the exception of slightly lower cross-measure correlation values.

3.1.2 Contributions of baseline connectivity

Prior ECoG literature (Kramer et al., 2011; Fox et al., 2018; Kucyi et al., 2018; Mostame et al., 2019) suggests the existence of an intrinsic connectivity architecture, the organization of which is largely preserved independent of whether or not an external stimulus or cognitive demand is being processes. In the following, we use "intrinsic" to refer to a spatial FC organization that is reflective of a task-independent functional architecture and/or contains contributions from stimulus-independent sustained task-set maintenance (Dosenbach et al., 2006). To determine the extent to which the observed spatial relationship between PhC and AmpC post-stimulus FC matrices is driven by stimulus processing or an intrinsic organization, we assessed spatial correlation across PhC and AmpC FC matrices of the pre-stimulus interval for all frequency bands. Interestingly, substantial spatial correlation between the two coupling modes was detected similar to the findings in the post-stimulus interval (dashed gray line in Fig. 6B). This similarity across pre- and post-stimulus intervals implies that the significant cross-measure correlation was not generated solely by stimulus processing but rather is suggestive of an intrinsic FC organization.

To further corroborate this observation, we investigated the cross-measure spatial similarity of *task-evoked* static FC derived by subtracting the pre-stimulus static FC matrices from corresponding post-stimulus static FC matrices. In other words, we removed the proportion of FC (separately for both PhC and AmpC) that was consistent across pre- and post-stimulus conditions. The cross-measure correlation values for task-evoked FC dropped substantially in comparison to the post-stimulus condition in all individual subjects (Fig. 6B; group-level *t*-test of dashed orange line vs. black line: $t_{theta,17}$ = 15.88 (p=6.21e-12), $t_{alpha,17}$ = 15.80 (p=6.80e-12), $t_{beta,17}$ = 13.13 (p=1.25e-10), $t_{gamma,17}$ = 10.90 (p=2.14e-9), $t_{high\ gamma,17}$ = 11.08 (p=1.68e-9)). To

summarize, the substantially reduced cross-measure similarity in all frequencies and all single subjects (orange vs. black data) suggests that high spatial correlation between PhC and AmpC is generated by an intrinsic FC organization irrespective of presence or absence of trial-related cognitive processes.

Note that because electrode distance can impact both PhC and AmpC, thereby inflating the spatial correlation between the two coupling modes, we replicated the results of Fig. 6B after regressing out distance dependencies from each FC measure (Fig. 6C). Although Fig. 6C shows slightly lower values for cross-measure correlations, major conclusions from Fig. 6B remained valid. FC in PhC and AmpC correlated in the range of R =0.39 to 0.19 for post-stimulus condition, gradually decreasing with increasing frequency. Again, these spatial correlations already existed during the pre-stimulus interval (Fig. 6C; gray line), indicating that the cross-measure spatial similarity is not driven by task processing. When assessing the task-evoked cross-measure spatial correlation, a significant drop compared to the corresponding R values of post-stimulus intervals was detected (Fig. 6C; group-level t-test of dashed orange line vs. black line: $t_{theta,17}$ = 11.08 (p=1.69e-9), $t_{alpha,17}$ = 11.20 (p=1.43e-9), $t_{beta,17}$ = 7.35 (p=5.67e-7), $t_{gamma,17}$ = 6.63 (p=2.14e-6), $t_{high\ gamma,17}$ = 7.48 (p=4.51e-7)). This consistency indicates that the observed spatial similarity between PhC and AmpC is not driven entirely by distance dependencies and reflects an inherent property of FC in the brain.

3.1.3 Contributions of volume conduction effects

It is known that volume conduction is dependent on electrode distance (Rouse et al., 2016; Dubey and Ray, 2019; Rogers et al., 2019). Therefore, the persistence of effects after distance regression tentatively speaks against volume conduction driving the cross-measure similarities. We confirmed that volume conduction is not the primary source of the effects by demonstrating

significant spatial relationship between PhC and AmpC using two other FC measures, wPLI and ImC (supplementary data section 2). These measures suppress zero-lag connectivity, a common approach to exclude any potential contributions from volume conduction effects as leakage is assumed to propagate instantaneously (Palva and Palva, 2012). At the group level, we observed that cross-measure spatial correlations of all frequency bands were significantly greater than chance level (Supplementary data section 2). At single-subject level, the spatial correlation exceeded the null model in all 18 (subjects) × 5 (frequency bands) comparisons with few exceptions (Supplementary Fig. 11). To summarize, the FC organization of PhC and AmpC comprises spatial similarity not trivially explained by spurious volume conductance effects.

3.1.4 Static FC in an independent task

In the secondary dataset (verb generation task with 6 subjects), we made equivalent observations regarding the spatial correlation of PhC and AmpC during pre- and post- stimulus intervals (1.5s each) as well as their spatially divergent task-evoked changes (i.e. post- minus pre-stimulus FC). During processing of the trial (language processing), we found significant spatial correlations of roughly comparable magnitude as in the primary dataset in all subjects and for all frequency bands (Fig. 8A left side; black line, R = 0.52 to 0.38). The spatial correlation between PhC and AmpC was significant for all individual subjects and frequency bands ($q < 0.005$ corrected for 30 (5 frequencies × 6 subjects) multiple comparisons by Benjamini-Hochberg method). Again, these spatial correlations already existed during the pre-stimulus interval (Fig. 8A left side; gray line), indicating that the cross-measure spatial similarity is not driven by task processing. When assessing the spatial correlation between static task-evoked PhC and AmpC changes, a significant drop compared to the corresponding R values of post-stimulus intervals was detected in all individual subjects (Fig. 8A left side; orange vs. black data points). Further, these

observations largely persisted after removing the impact of distance from both measures (Fig. 8A right side). Confirmation of findings in the verb generation task establishes independence of the cross-measure spatial similarity and its intrinsic nature from particular task demands.

To summarize results of section 3.1, the spatial organization of PhC and AmpC is strongly correlated, especially for lower frequencies, and this correlation dissipates almost fully after subtraction of pre-stimulus coupling. The latter observation supports the view that the spatial correlation across the two connectivity measures is largely driven by an intrinsically maintained FC organization present in both measures, especially in lower frequency bands. The low spatial correlation between uniquely task-evoked (i.e. baseline-corrected) FC organization across the two coupling modes implies that PhC and AmpC do not increase/decrease together from baseline in a manner that is consistent across connections, at least when assessed in a static fashion over the 2.5s (1.5s for secondary data) post-stimulus period. This observation encouraged us to investigate the linear temporal relationship of task-evoked FC changes, or dynamics, over the course of stimulus processing.

3.2 Dynamic framework

In the following, we assess whether time-varying changes in one FC measure co-occurred with changes in the other measure during stimulus processing. For each electrode pair, using sliding windows, the *timecourses* of PhC and AmpC were calculated as phase lag consistency over trials or as Pearson correlations of the Hilbert amplitude, respectively. Timecourses of both measures were normalized to the corresponding 0.5s pre-stimulus baseline. The sliding window and baseline-normalization mirror typical cognitive neuroscience approaches (Sederberg et al., 2003; Hanslmayr et al., 2007; Schölvinck et al., 2013). Note that co-fluctuation in PhC and AmpC in a given connection over time does not determine the presence or the sign of static connectivity in

either FC measure at that connection. Consequently, the dynamic framework is independent of the arrangement of static FC over connections and the cross-measure spatial correlation of this arrangement reported in the static framework, especially if the cross-measure co-dynamics varies over connections.

3.2.1 Spatial characterization of task-involvement

Here, we sought to assess whether PhC and AmpC changes linked to trial-related processes co-occur across the same region pairs. To determine which electrode pairs show increase/decrease in PhC (respectively AmpC) during stimulus processing, we tested the difference between dynamic FC averaged over 500ms pre- and post-stimulus intervals for each electrode pair (pooled *t*-test, Benjamini-Hochberg FDR-corrected for all electrode pairs for each subject, $q < 0.01$). Fig. 7 depicts the number of electrode pairs showing different logical combinations of significant changes in PhC and AmpC relative to pre-stimulus baseline: I) PhC II) AmpC III) PhC AND AmpC IV) PhC XOR AmpC V) PhC OR AmpC.

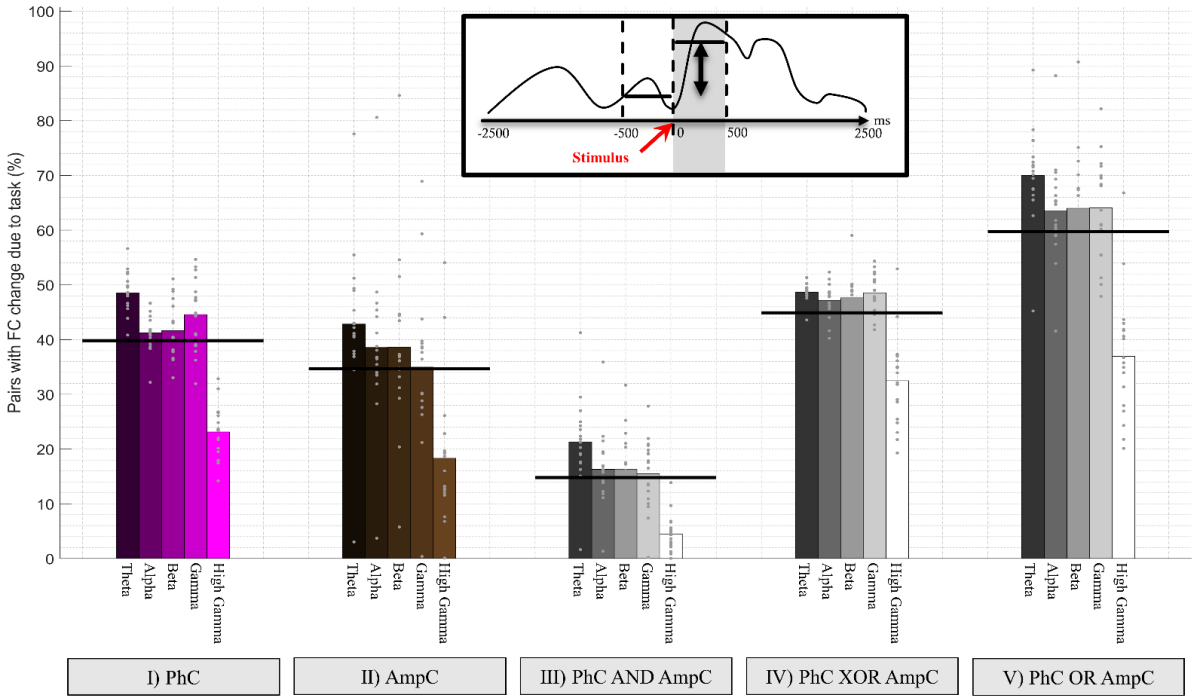

Fig. 7 - Proportion of electrode pairs showing significant FC changes due to task in 5 logical combinations of PhC and AmpC – Changes detected in I) PhC, II) AmpC, III) both of the measures (AND), IV) exclusively one of the measures (XOR), and V) at least one of the measures (OR), over all frequency bands. Dots show single subject percentages while bars show average of the percentages over subjects. Black horizontal lines represent mean over frequencies for each combination. While a relatively large number of electrode pairs showed task-related FC change in at least one coupling mode (combination V), only a small proportion of electrodes did so in both coupling modes concurrently (combination III), suggesting that the temporal dynamics of the two coupling modes diverge during task processing.

We observed a qualitative difference between mean number of connections in combinations I and II pooled over all frequencies and subjects. This result may imply that PhC is more strongly involved in task processing (i.e. task-evoked FC changes from baseline), suggesting that task-evoked FC employs phase-based connectivity more extensively than amplitude-based connectivity (note however that we cannot exclude a contribution from potentially different signal to noise ratios of PhC and AmpC). Combination III shows that only about 15% of electrode pairs exhibit significant FC changes due to task in both coupling modes, implying that the two modes are not identical to each other. The high values in combination IV show that a

large percentage of electrode pairs diverge in task-evoked FC changes such that change in one coupling mode is not accompanied by the other. From these observations, it can be inferred that PhC and AmpC provide spatially divergent and thus dissociable coupling modes in terms of task-related time-varying FC. This observation motivates to directly investigate the degree to which time-varying PhC and AmpC dynamics co-evolve over the course of stimulus processing, i.e. whether or not their timecourses exhibit linear temporal dependencies.

3.2.2 Temporal correlations of FC dynamics

To quantify the degree to which the dynamic timecourses of PhC and AmpC co-vary with each other, we estimated Pearson correlation between the two modes for every electrode pair (restricted to electrode pairs exhibiting significant FC change due to the stimulus in at least one of the two measures (Fig. 7. combination V separately for each frequency band)). We assessed the statistical significance of this co-variation for each electrode pair against a null model that phase-randomized the two FC timecourses (see Fig. 5; $q < 0.05$, Benjamini-Hochberg FDR-corrected). We quantified the percentage of positively correlated, anticorrelated, and uncorrelated dynamics over all electrode pairs for all frequency bands (Table 1; averaged over subjects). Surprisingly, we observed that task-evoked dynamics of PhC and AmpC are largely uncorrelated over time for all frequency bands (i.e. statistically indistinguishable from null). PhC and AmpC task-evoked time-varying FC were temporally uncorrelated in ~99% of the electrode pairs (percentage averaged over subjects and across all bands). The small proportion of remaining electrode pairs showed either positively or negatively correlated time-varying FC across the two coupling modes. Moreover, the temporal correlations between PhC and AmpC time-varying FC across all electrode pairs had a symmetric histogram centered around zero similarly to the null histogram, indicating that PhC and AmpC dynamics are not linearly

correlated in either positive or negative directions in a systematic way (Single subject sample shown in Fig. 10).

Table 1 – Percentage of electrode pairs showing anti-correlated, uncorrelated, and positively correlated PhC and AmpC time-varying FC in the epoched data (sub-columns). First row shows the results of the primary dataset while the second row shows corresponding results of the secondary dataset. Each column corresponds to one frequency band. Values show the percentage averaged across all subjects (±SD). The vast majority of electrode pairs show no linear correlation between PhC and AmpC time-varying dynamics in any frequency band.

	Theta			Alpha			Beta			Gamma			High gamma		
Effect	Negative	Uncorrelated	positive	Negative	Uncorrelated	positive	Negative	Uncorrelated	positive	Negative	Uncorrelated	positive	Negative	Uncorrelated	positive
Grand Average (%) Primary data (Motor task)	0.1 (±0.0)	99.5 (±0.4)	0.4 (±0.4)	0.2 (±0.2)	98.8 (±0.6)	1.0 (±0.6)	0.2 (±0.3)	98.9 (±0.7)	0.8 (±0.6)	0.3 (±0.2)	99.0 (±0.3)	0.7 (±0.3)	0.2 (±0.2)	98.8 (±1.5)	1.0 (±1.5)
Grand Average (%) Secondary data (Speech task)	1.0 (±0.4)	97.6 (±0.5)	1.4 (±0.2)	0.7 (±0.4)	98.3 (±0.4)	1.0 (±0.2)	0.7 (±0.2)	98.4 (±0.4)	0.9 (±0.3)	0.7 (±0.1)	98.3 (±0.5)	1.0 (±0.4)	0.3 (±0.2)	97.2 (±3.3)	2.5 (±3.3)

To ensure that the low temporal association between PhC and AmpC dynamics is not driven by inadequately short window length (post-stimulus interval of 2.5s) or limited number of data points, we additionally tested the linear temporal correspondence of PhC and AmpC in the continuous data (analysis details provided in supplementary materials). For each electrode pair and frequency band, we extracted PhC and AmpC timecourses from the continuous data and estimated temporal correlation between them within a window sliding over time (Fig. 9; The window length was determined in a data driven fashion with an average length of ~=58s across

subjects and frequency bands). Applying the same procedure as was used for the epoched data (see Fig. 5), we tested the significance of the temporal correlations between PhC and AmpC for each electrode pair within each time window. Results are shown for the continuous data in Table 2. We found that ~99% of all correlation values across all electrode pairs and time windows did not exceed chance level. Similar to the epoched data, the temporal correlation values were distributed symmetrically around zero, indicating the absence of any systematic linear dependence between PhC and AmpC temporal dynamics (Fig. 10). In line with the findings from the epoched data, it can be concluded that PhC and AmpC time-varying dynamics are distinguishable from each other.

3.2.3 Temporally resolved FC in the secondary dataset

In the secondary dataset, we made equivalent observations regarding the percentage of electrode pairs with significant change due to task execution (Fig. 8B). Similar to the primary dataset, trial-related FC changes converged over PhC and AmpC only on ~15% of electrode pairs indicating the dissociability of the two coupling modes (Contrast III). Moreover, contrast IV implies that around 46% of electrode pairs show diverging PhC and AmpC task-related time-varying FC. Altogether, these observations support the conclusion that task-related spatial reorganization of time-varying PhC and AmpC largely diverge.

Paralleling analyses of the primary dataset, we further assessed the temporal correlation of PhC and AmpC timecourses (see section 2.3.1 & 2.3.2). Again, the vast majority of electrode pairs (~98%) showed temporal independence of PhC and AmpC dynamics in all frequency bands in both the active trial periods (Table 1) and the continuous data (Table 2). This outcome further confirms that PhC and AmpC are two dissociable modes of coupling.

Table 2 – Same as Table. 1 but for continuous data (see supplementary materials for analysis details). The vast majority of electrode pairs show uncorrelated PhC and AmpC time-varying dynamics in both primary and secondary datasets.

	Theta			Alpha			Beta			Gamma			High gamma		
Effect	Negative	Uncorrelated	positive	Negative	Uncorrelated	positive	Negative	Uncorrelated	positive	Negative	Uncorrelated	positive	Negative	Uncorrelated	positive
Grand Average (%) Primary data (Motor task)	0.1 (±0.0)	99.2 (±0.2)	0.7 (±0.2)	0.1 (±0.0)	99.3 (±0.2)	0.6 (±0.2)	0.1 (±0.0)	99.3 (±0.2)	0.6 (±0.2)	0.1 (±0.0)	99.5 (±0.1)	0.4 (±0.1)	0.1 (±0.0)	98.8 (±1.9)	1.1 (±1.9)
Grand Average (%) Secondary data (Speech task)	0.1 (±0.1)	99.2 (±0.2)	0.5 (±0.2)	0.1 (±0.0)	99.3 (±0.2)	0.6 (±0.2)	0.1 (±0.0)	99.4 (±0.1)	0.5 (±0.1)	0.1 (±0.1)	99.4 (±0.2)	0.5 (±0.1)	0.1 (±0.1)	99.0 (±0.7)	0.9 (±0.7)

To summarize results of section 3.2, PhC and AmpC exhibit distinct task-related time-varying FC changes across electrode pairs. This divergence is due to largely independent temporal dynamics of the two coupling modes over the course of time. These findings imply that PhC and AmpC are two dissociable modes of coupling despite their spatial similarity reported in section 3.1.

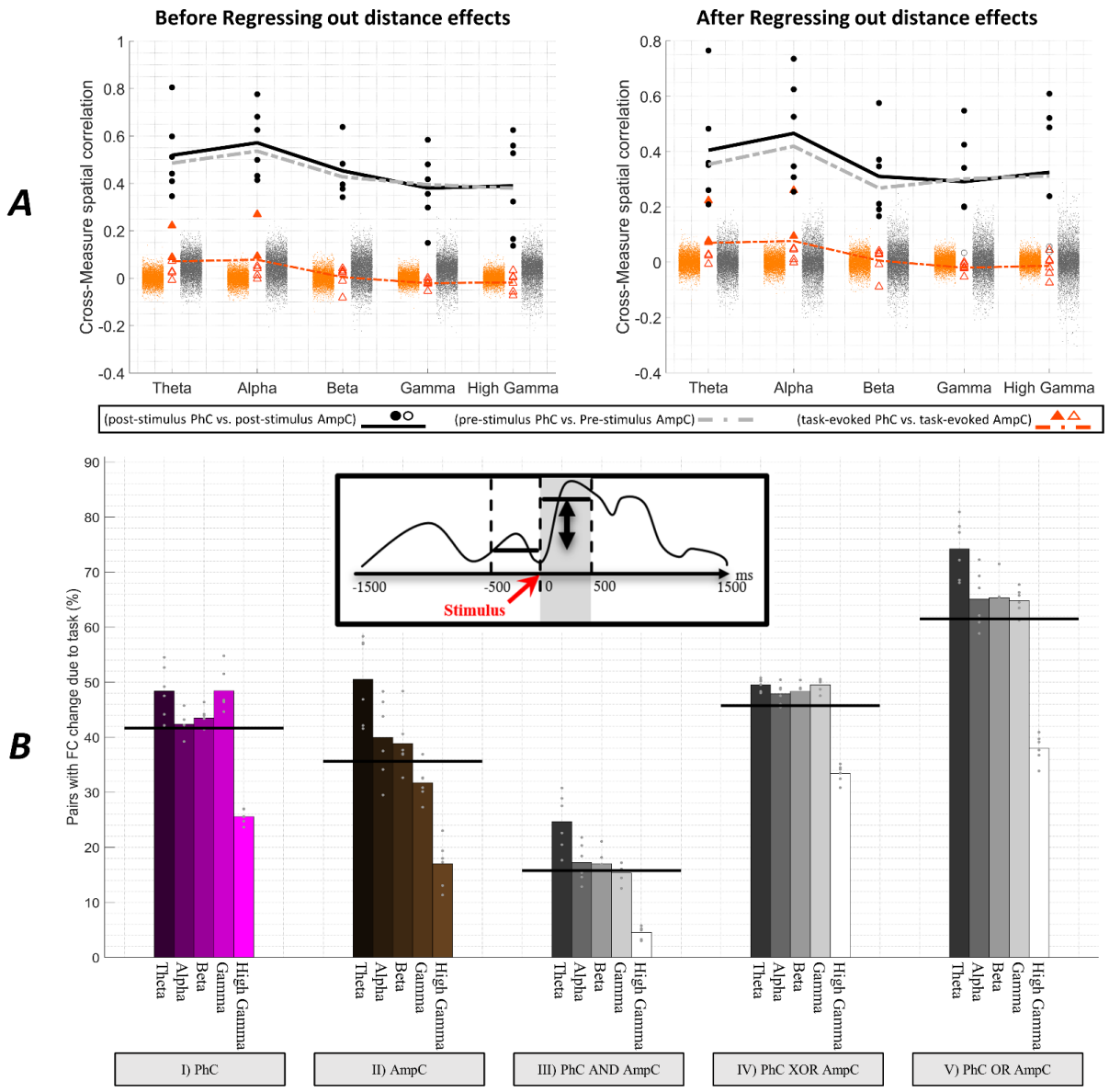

Fig. 8 – Findings of Fig. 6 & 7 extended to a second ECoG dataset of 6 subjects performing a verb generation task - A) Spatial correlation between PhC and AmpC in the secondary dataset before (left panel) and after (right panel) regressing out distance dependencies. Visualization and color code are equivalent to Fig. 6B-C. Significant difference of PhC-to-AmpC spatial correlation between the post-stimulus and task-evoked conditions (black vs. orange) confirms that the observed spatial correspondence of PhC and AmpC is due to an intrinsic spatial organization (cf. Fig. 6). B) Percentage of electrode pairs showing significant change in their FC dynamics due to language processing in the secondary dataset shown for all frequency bands. Results are shown for five logical contrasts in an arrangement equivalent to Fig. 7. Task-evoked temporally resolved PhC and AmpC occur in largely divergent electrode pairs, confirming findings of the primary dataset (cf. Fig. 7).

CHAPTER 4: DISCUSSION

Functional connectivity in neurophysiological signals has been estimated in the literature using measures of two biologically different coupling modes: synchronization of rhythmic activity cycles (PhC), and synchronization of activation amplitude (AmpC). This fundamental difference between PhC and AmpC measures may result in crucially different observations. Nevertheless, previous studies have commonly investigated one or the other type of FC mode without full knowledge of their relationship. Here, we assessed the correspondence and differences across PhC and AmpC by investigating their spatial (static FC analyses) and temporal (dynamic FC analyses) organization. Here, we report a strong and intrinsically maintained spatial relationship across PhC and AmpC. We further show that additional FC modulation during motor and language process spatially and temporally diverge across PhC and AmpC. The findings highlight both the close association and the dissociability of the two coupling modes.

In the static framework, we found significant spatial correlation across the topography of PhC and AmpC during stimulus processing in all frequency bands (R=0.50 to 0.31). Recent simulation work suggests the intriguing possibility that PhC and AmpC may both be functions of lagged coherence for Gaussian distributed data (Nolte et al., 2019), which could explain the spatial similarity observed in our study. On the other hand, rare behavioral studies that investigate both PhC and AmpC in the same task context conclude that the two distinct coupling modes are involved in different cortical computations (Helfrich et al., 2016). This observation speaks against the two modes being reflective of the same underlying connectivity. Supporting this latter view, the almost complete temporal independence across PhC and AmpC timecourses in both of our datasets (Tables 1 and 2) suggests that they reflect two dissociable modes of functional connectivity.

Interestingly, the spatial correlation between PhC and AmpC vanished almost entirely when accounting for FC present prior to stimulus onset. This observation suggests that both measures capture a connectivity organization that is intrinsically present independent of external stimulation (convergence of PhC and AmpC). As shown in Fig. 6B, the correlation between the spatial organization of PhC and AmpC stemmed from a portion of FC organization consistent over pre- and post-stimulus periods. What constitutes this consistent FC portion? One possibility is contributions from continuous and intrinsically driven maintenance of task-set (Dosenbach et al., 2006), comprising sustained attentional and preparatory processes, and the maintenance of task rules and stimuli.

Another and in our view more probable explanation is a task-independent ongoing FC organization spanning mental states. Over the past decade, numerous fMRI studies have shown that the spatial organization of FC remains largely intact in the presence of stimulation or cognitive challenges when compared to task-free resting state (Cole et al., 2014; Krienen et al., 2014; Gratton et al., 2018). Recent surface EEG/MEG and intracranial EEG studies have demonstrated the presentence of a similar FC organization in neurophysiological PhC or AmpC at least during task-free resting state (Brookes et al., 2011; Sockeel et al., 2016; Kucyi et al., 2018). This observation suggests that there exists a task-independent intrinsic "cognitive architecture" (Petersen and Sporns, 2015) persisting over different mental states. Therefore, the high spatial correlation between PhC and AmpC could reflect the presence of this architecture in both FC modes. Note that this intrinsic architecture might be partially reflecting the structural connectivity that is beyond the scope of this study (Finger et al., 2016; Wirsich et al., 2017).

Importantly, beyond the persistent intrinsic FC organization, additional PhC and AmpC changes unfold during the active trial that spatially and temporally diverge between the two coupling

modes. As described above, the PhC-AmpC spatial correspondence did not further increase from its pre-stimulus level during the active trial. This finding indicates that trial-related PhC and AmpC changes occur in a spatially independent manner. We further solidified this observation by assessing whether the same electrode pairs showed trial-related FC changes in PhC and AmpC. We found that ~60% of connections showed FC change in PhC or AmpC compared to pre-stimulus baseline, but only ~15% showed changes in both modes (average over frequencies and subjects). These observations point to spatial divergence of trial-related FC changes across AmpC and PhC. This conclusion is in line with the proposal that the two coupling modes fulfil dissociable functions in the service of tasks (Engel et al., 2013).

In a second step, we asked whether dynamic trial-related FC changes of PhC and AmpC linearly co-evolve over the course of the trial. We found that the timecourses of PhC and AmpC are largely linearly independent of each other (from gamma through theta bands, we found only ~2% of electrode pairs with a temporal relationship higher than the null model). To ensure that the temporal independence between PhC and AmpC did not stem from the limited trial interval, we confirmed the null result in continuous data encompassing both trials and the inter-trial intervals. Although future studies are needed to assess whether there may exist non-linear or time-lagged temporal associations between PhC and AmpC (similarly to what has been shown for phase *lag* and AmpC (Womelsdorf et al., 2007)), our observations indicate the almost complete absence of a linear temporal relationship. This temporal divergence further corroborates the observation that PhC and AmpC represent two dissociable FC modes for encoding task-related information.

Our findings were confirmed in a second task (6 subjects). Importantly, the extension to a cognitively demanding task supports the independence of the outcomes from the cognitive/behavioral domain (motor versus language task). To ensure that our observations were

not largely driven by volume conduction effects, we further replicated them based on ImC and wPLI measures of PhC which suppress zero-lag connectivity (Nolte et al., 2004; Vinck et al., 2011). For both alternative measures, we confirmed 1) the significant PhC-to-AmpC spatial similarity during the post-stimulus period, and 2) the significant reduction of this similarity from post-stimulus to task-evoked conditions. These replications with wPLI and ImC measures speak against volume conduction effects as the primary source of the cross-measure correlation. However, the effect diminished in magnitude compared to the initial PLV-based results, especially in lower frequency bands. This drop in R values is likely due to the underestimation of FC resulting from suppression of real zero-lag connectivity (Bastos and Schoffelen, 2016). Converging evidence from both human scalp EEG (Rodriguez et al., 1999) and intracranial animal electrophysiology (e.g., Gray et al. 1989; Roelfsema et al. 1997), structure-function comparisons (e.g., Finger et al. 2016), and simulation studies (Viriyopase et al., 2012) indeed supports the existence and mechanistic relevance of veridic zero-lag long-range FC. The conservative suppression of the latter thus likely reduced but did not abolish the spatial correspondence between PhC and AmpC. Altogether, we conclude that our findings are largely generalizable across different cognitive tasks, FC measures, and individual brains.

Limitations

ECoG provides superb signal-to-noise ratio and spatial resolution compared to non-invasive scalp recordings. However, these unparalleled qualities come at the cost of incomplete spatial coverage. In this study, we used ECoG signals of total 20 subjects with electrode grids mainly covering fronto-temporal brain regions. Thus, all observations are limited to connections among the covered areas. Due to this spatial limitation we could not assess the correspondence of our findings, especially the intrinsically present FC organization, to the well-known neurocognitive

connectivity networks (default mode network, dorsal attention network etc.). Future studies may be able to address this limitation by integrating ECoG with surface EEG/MEG literature, or using ECoG signals from non-human primates with more comprehensive coverage (Hindriks et al., 2018). Importantly, comparable results across individuals with differing electrode coverage supports the general nature of the observations irrespective of the specific brain regions covered.

Another limitation stems from the necessity of using the absolute value of AmpC in order to make the range of this measure comparable to that of PhC. Consequently, we could only compare PhC with strength of AmpC rather than with the sign of AmpC. Therefore, our approach cannot answer how negatively correlated versus positively correlated signal envelopes may distinctly relate to PhC.

Finally, we note that there are other important coupling modes that bridge *across* frequencies and are beyond the scope of the current investigations (Canolty et al., 2010; Palva and Palva, 2018). As a prominent example, in cross-frequency phase-amplitude coupling the phase of a relatively slow oscillation (e.g. theta or alpha) is tied to the amplitude of a faster rhythm (e.g. gamma). Phase-amplitude coupling is particularly functionally important for modulatory influences (via phase cycle) onto lower-order brain processes (represented by high-frequency amplitude fluctuations) (Szczepanski et al., 2014), and for separating spatially distributed networks that work in parallel (Meij et al., 2012). Coupling of phase and amplitude can occur within the same brain region (e.g. R. T. Canolty et al. 2006; Szczepanski et al. 2014). Alternatively, the amplitude of a rhythm in one region can be coupled to the phase of another frequency in another region (e.g. Ryan T. Canolty et al. 2010; Meij, Kahana, and Maris 2012). In the latter case, phase-amplitude coupling provides a separate means of FC beyond PhC and AmpC. In the former case, if phase-amplitude coupling occurs in different brain regions at a similar cycle of

the phase-providing frequency (i.e. concurrently expressing PhC), it could provide a mechanistic explanation for the spatial similarity that we report between static PhC and AmpC in the current study. These intriguing scenarios call for future investigations into a potential link between cross-frequency processes and the PhC-to-AmpC relationship assessed in the current work.

CHAPTER 5: CONCLUSION

Neural connectivity may be achieved by two theoretically distinct coupling modes, one involving the timing of rhythmic neural firing (PhC) and the other the number of neurons firing in a given rhythm (AmpC). This conceptual proposal (Engel et al., 2013; Schölvinck et al., 2013) calls for quantitative empirical comparison of the two FC modes in terms of their spatial and temporal relationship. Using the superb spatial resolution and signal-to-noise ratio of ECoG data, our findings show that the brain indeed implements FC using both coupling modes. On the one hand, PhC and AmpC are intrinsically organized in a highly similar spatial pattern that is unmodulated by externally evoked neural processes. On the other hand, spatial organization and temporal evolution of trial-evoked PhC and AmpC do not converge. We conclude that the brain may employ the two coupling modes in a distinct manner to meet task demands. PhC and AmpC thus provide the basis for parallel and independent neural "conversations". These findings help to integrate the disconnected electrophysiology literature using measures of PhC versus AmpC and lead to two major implications. Firstly, PhC and AmpC analyses of future task-based studies may need to account for the existence of an intrinsic spatial FC organization that persists throughout baseline and stimulus periods. Secondly, the observations suggest that neurophysiological FC studies will be most informative if they investigate both PhC and AmpC, as the two measures provide spatially and temporally distinct and complimentary information especially during cognitive tasks.

REFERENCES

Bastos AM, Schoffelen J-M (2016) A tutorial review of functional connectivity analysis methods and their interpretational pitfalls. Front Syst Neurosci 9:175.

Betzel RF, Medaglia JD, Kahn AE, Soffer J, Schonhaut DR, Bassett DS (2019) Structural, geometric and genetic factors predict interregional brain connectivity patterns probed by electrocorticography. Nat Biomed Eng:1.

Biswal B, Zerrin Yetkin F, Haughton VM, Hyde JS (1995) Functional connectivity in the motor cortex of resting human brain using echo-planar mri. Magn Reson Med 34:537–541.

Brookes MJ, Gibson AM, Hall SD, Furlong PL, Barnes GR, Hillebrand A, Singh KD, Holliday IE, Francis ST, Morris PG (2005) GLM-beamformer method demonstrates stationary field, alpha ERD and gamma ERS co-localisation with fMRI BOLD response in visual cortex. NeuroImage 26:302–308.

Brookes MJ, Woolrich M, Luckhoo H, Price D, Hale JR, Stephenson MC, Barnes GR, Smith SM, Morris PG (2011) Investigating the electrophysiological basis of resting state networks using magnetoencephalography. Proc Natl Acad Sci 108:16783–16788.

Canolty RT, Edwards E, Dalal SS, Soltani M, Nagarajan SS, Kirsch HE, Berger MS, Barbaro NM, Knight RT (2006) High Gamma Power Is Phase-Locked to Theta Oscillations in Human Neocortex. Science 313:1626–1628.

Canolty RT, Ganguly K, Kennerley SW, Cadieu CF, Koepsell K, Wallis JD, Carmena JM (2010) Oscillatory phase coupling coordinates anatomically dispersed functional cell assemblies. Proc Natl Acad Sci 107:17356–17361.

Cohen MX (2015) Effects of time lag and frequency matching on phase-based connectivity. J Neurosci Methods 250:137–146.

Colclough GL, Woolrich MW, Tewarie PK, Brookes MJ, Quinn AJ, Smith SM (2016) How reliable are MEG resting-state connectivity metrics? NeuroImage 138:284–293.

Cole MW, Bassett DS, Power JD, Braver TS, Petersen SE (2014) Intrinsic and task-evoked network architectures of the human brain. Neuron 83:238–251.

De Pasquale F, Della Penna S, Snyder AZ, Lewis C, Mantini D, Marzetti L, Belardinelli P, Ciancetta L, Pizzella V, Romani GL (2010) Temporal dynamics of spontaneous MEG activity in brain networks. Proc Natl Acad Sci 107:6040–6045.

Deligianni F, Centeno M, Carmichael DW, Clayden JD (2014) Relating resting-state fMRI and EEG whole-brain connectomes across frequency bands. Front Neurosci 8:258.

Dosenbach NUF, Visscher KM, Palmer ED, Miezin FM, Wenger KK, Kang HC, Burgund ED, Grimes AL, Schlaggar BL, Petersen SE (2006) A core system for the implementation of task sets. Neuron 50:799–812.

Dubey A, Ray S (2019) Cortical Electrocorticogram (ECoG) Is a Local Signal. J Neurosci 39:4299–4311.

Engel AK, Gerloff C, Hilgetag CC, Nolte G (2013) Intrinsic Coupling Modes: Multiscale Interactions in Ongoing Brain Activity. Neuron 80:867–886.

Fell J, Axmacher N (2011) The role of phase synchronization in memory processes. Nat Rev Neurosci 12:105–118.

Finger H, Bönstrup M, Cheng B, Messé A, Hilgetag C, Thomalla G, Gerloff C, König P (2016) Modeling of large-scale functional brain networks based on structural connectivity from DTI: comparison with EEG derived phase coupling networks and evaluation of alternative methods along the modeling path. PLoS Comput Biol 12:e1005025.

Fox KC, Foster BL, Kucyi A, Daitch AL, Parvizi J (2018) Intracranial electrophysiology of the human default network. Trends Cogn Sci.

Fox MD, Snyder AZ, Vincent JL, Corbetta M, Essen DCV, Raichle ME (2005) The human brain is intrinsically organized into dynamic, anticorrelated functional networks. Proc Natl Acad Sci 102:9673–9678.

Friston KJ (1994) Functional and effective connectivity in neuroimaging: A synthesis. Hum Brain Mapp 2:56–78.

Gabor D (1946) Theory of communication. Part 1: The analysis of information. J Inst Electr Eng - Part III Radio Commun Eng 93:429–441.

Gandal MJ, Edgar JC, Klook K, Siegel SJ (2012) Gamma synchrony: Towards a translational biomarker for the treatment-resistant symptoms of schizophrenia. Neuropharmacology 62:1504–1518.

Gordon SM, Franaszczuk PJ, Hairston WD, Vindiola M, McDowell K (2013) Comparing parametric and nonparametric methods for detecting phase synchronization in EEG. J Neurosci Methods 212:247–258.

Gratton C, Laumann TO, Nielsen AN, Greene DJ, Gordon EM, Gilmore AW, Nelson SM, Coalson RS, Snyder AZ, Schlaggar BL, Dosenbach NUF, Petersen SE (2018) Functional Brain Networks Are Dominated by Stable Group and Individual Factors, Not Cognitive or Daily Variation. Neuron 98:439-452.e5.

Gray CM, König P, Engel AK, Singer W (1989) Oscillatory responses in cat visual cortex exhibit inter-columnar synchronization which reflects global stimulus properties. Nature 338:334–337.

Greenblatt RE, Pflieger ME, Ossadtchi AE (2012) Connectivity measures applied to human brain electrophysiological data. J Neurosci Methods 207:1–16.

Greicius MD, Krasnow B, Reiss AL, Menon V (2003) Functional connectivity in the resting brain: A network analysis of the default mode hypothesis. Proc Natl Acad Sci 100:253–258.

Hacker CD, Snyder AZ, Pahwa M, Corbetta M, Leuthardt EC (2017) Frequency-specific electrophysiologic correlates of resting state fMRI networks. NeuroImage 149:446–457.

Hanslmayr S, Aslan A, Staudigl T, Klimesch W, Herrmann CS, Bäuml K-H (2007) Prestimulus oscillations predict visual perception performance between and within subjects. NeuroImage 37:1465–1473.

Helfrich RF, Knepper H, Nolte G, Sengelmann M, König P, Schneider TR, Engel AK (2016) Spectral fingerprints of large-scale cortical dynamics during ambiguous motion perception. Hum Brain Mapp 37:4099–4111.

Hillebrand A, Barnes GR, Bosboom JL, Berendse HW, Stam CJ (2012) Frequency-dependent functional connectivity within resting-state networks: an atlas-based MEG beamformer solution. Neuroimage 59:3909–3921.

Hindriks R, Micheli C, Bosman CA, Oostenveld R, Lewis C, Mantini D, Fries P, Deco G (2018) Source-reconstruction of the sensorimotor network from resting-state macaque electrocorticography. NeuroImage 181:347–358.

Hipp JF, Hawellek DJ, Corbetta M, Siegel M, Engel AK (2012) Large-scale cortical correlation structure of spontaneous oscillatory activity. Nat Neurosci 15:884.

Kopell N, Ermentrout GB, Whittington MA, Traub RD (2000) Gamma rhythms and beta rhythms have different synchronization properties. Proc Natl Acad Sci 97:1867–1872.

Kramer MA, Eden UT, Lepage KQ, Kolaczyk ED, Bianchi MT, Cash SS (2011) Emergence of Persistent Networks in Long-Term Intracranial EEG Recordings. J Neurosci 31:15757–15767.

Krienen FM, Yeo BT, Buckner RL (2014) Reconfigurable task-dependent functional coupling modes cluster around a core functional architecture. Philos Trans R Soc B Biol Sci 369:20130526.

Kucyi A, Schrouff J, Bickel S, Foster BL, Shine JM, Parvizi J (2018) Intracranial Electrophysiology Reveals Reproducible Intrinsic Functional Connectivity within Human Brain Networks. J Neurosci 38:4230–4242.

Lachaux J-P, Rodriguez E, Martinerie J, Varela FJ (1999) Measuring phase synchrony in brain signals. Hum Brain Mapp 8:194–208.

Meij R van der, Kahana M, Maris E (2012) Phase–Amplitude Coupling in Human Electrocorticography Is Spatially Distributed and Phase Diverse. J Neurosci 32:111–123.

Miller KJ (2019) A library of human electrocorticographic data and analyses. Nat Hum Behav 3:1225–1235.

Miller KJ, Abel TJ, Hebb AO, Ojemann JG (2011) Rapid online language mapping with electrocorticography. J Neurosurg Pediatr 7:482–490.

Miller KJ, Leuthardt EC, Schalk G, Rao RPN, Anderson NR, Moran DW, Miller JW, Ojemann JG (2007) Spectral Changes in Cortical Surface Potentials during Motor Movement. J Neurosci 27:2424–2432.

Mitra PP, Pesaran B (1999) Analysis of Dynamic Brain Imaging Data. Biophys J 76:691–708.

Mostame P, Moharramipour A, Hossein-Zadeh G-A, Babajani-Feremi A (2019) Statistical Significance Assessment of Phase Synchrony in the Presence of Background Couplings: An ECoG Study. Brain Topogr Available at: https://doi.org/10.1007/s10548-019-00718-8 [Accessed July 8, 2019].

Nolte G, Bai O, Wheaton L, Mari Z, Vorbach S, Hallett M (2004) Identifying true brain interaction from EEG data using the imaginary part of coherency. Clin Neurophysiol 115:2292–2307.

Nolte G, Galindo-Leon E, Li Z, Liu X, Engel AK (2019) Mathematical relations between measures of brain connectivity estimated from electrophysiological recordings for Gaussian distributed data. bioRxiv:680678.

O'Neill GC, Bauer M, Woolrich MW, Morris PG, Barnes GR, Brookes MJ (2015) Dynamic recruitment of resting state sub-networks. NeuroImage 115:85–95.

Oostenveld R, Fries P, Maris E, Schoffelen J-M (2011) FieldTrip: Open Source Software for Advanced Analysis of MEG, EEG, and Invasive Electrophysiological Data. Intell Neurosci 2011:1:1-1:9.

Palva JM, Palva S (2018) Functional integration across oscillation frequencies by cross-frequency phase synchronization. Eur J Neurosci 48:2399–2406.

Palva JM, Wang SH, Palva S, Zhigalov A, Monto S, Brookes MJ, Schoffelen J-M, Jerbi K (2018) Ghost interactions in MEG/EEG source space: A note of caution on inter-areal coupling measures. NeuroImage 173:632–643.

Palva S, Palva JM (2012) Discovering oscillatory interaction networks with M/EEG: challenges and breakthroughs. Trends Cogn Sci 16:219–230.

Petersen SE, Sporns O (2015) Brain Networks and Cognitive Architectures. Neuron 88:207–219.

Prichard D, Theiler J (1994) Generating surrogate data for time series with several simultaneously measured variables. Phys Rev Lett 73:951–954.

Rodriguez E, George N, Lachaux J-P, Martinerie J, Renault B, Varela FJ (1999) Perception's shadow: long-distance synchronization of human brain activity. Nature 397:430–433.

Roelfsema PR, Engel AK, König P, Singer W (1997) Visuomotor integration is associated with zero time-lag synchronization among cortical areas. Nature 385:157–161.

Rogers N, Hermiz J, Ganji M, Kaestner E, Kılıç K, Hossain L, Thunemann M, Cleary DR, Carter BS, Barba D, Devor A, Halgren E, Dayeh SA, Gilja V (2019) Correlation Structure in Micro-ECoG Recordings is Described by Spatially Coherent Components. PLOS Comput Biol 15:e1006769.

Rouse AG, Williams JJ, Wheeler JJ, Moran DW (2016) Spatial co-adaptation of cortical control columns in a micro-ECoG brain–computer interface. J Neural Eng 13:056018.

Rubinov M, Sporns O (2010) Complex network measures of brain connectivity: Uses and interpretations. NeuroImage 52:1059–1069.

Sadaghiani S, Wirsich J (2019) Intrinsic connectome organization across temporal scales: New insights from cross-modal approaches. Netw Neurosci:1–49.

Schoffelen J-M, Gross J (2009) Source connectivity analysis with MEG and EEG. Hum Brain Mapp 30:1857–1865.

Schölvinck ML, Leopold DA, Brookes MJ, Khader PH (2013) The contribution of electrophysiology to functional connectivity mapping. NeuroImage 80:297–306.

Sederberg PB, Kahana MJ, Howard MW, Donner EJ, Madsen JR (2003) Theta and Gamma Oscillations during Encoding Predict Subsequent Recall. J Neurosci 23:10809–10814.

Singer W (2013) Cortical dynamics revisited. Trends Cogn Sci 17:616–626.

Singh KD, Barnes GR, Hillebrand A, Forde EME, Williams AL (2002) Task-Related Changes in Cortical Synchronization Are Spatially Coincident with the Hemodynamic Response. NeuroImage 16:103–114.

Sockeel S, Schwartz D, Pélégrini-Issac M, Benali H (2016) Large-scale functional networks identified from resting-state EEG using spatial ICA. PloS One 11:e0146845.

Stitt I, Galindo-Leon E, Pieper F, Engler G, Fiedler E, Stieglitz T, Engel AK (2015) Intrinsic coupling modes reveal the functional architecture of cortico-tectal networks. Sci Adv 1:e1500229.

Szczepanski SM, Crone NE, Kuperman RA, Auguste KI, Parvizi J, Knight RT (2014) Dynamic Changes in Phase-Amplitude Coupling Facilitate Spatial Attention Control in Fronto-Parietal Cortex. PLOS Biol 12:e1001936.

Tewarie P, Bright MG, Hillebrand A, Robson SE, Gascoyne LE, Morris PG, Meier J, Van Mieghem P, Brookes MJ (2016) Predicting haemodynamic networks using

electrophysiology: The role of non-linear and cross-frequency interactions. Neuroimage 130:273–292.

Uhlhaas P, Pipa G, Lima B, Melloni L, Neuenschwander S, Nikolić D, Singer W (2009) Neural synchrony in cortical networks: history, concept and current status. Front Integr Neurosci 3:17.

Uhlhaas PJ, Singer W (2012) Neuronal Dynamics and Neuropsychiatric Disorders: Toward a Translational Paradigm for Dysfunctional Large-Scale Networks. Neuron 75:963–980.

Varela F, Lachaux J-P, Rodriguez E, Martinerie J (2001) The brainweb: phase synchronization and large-scale integration. Nat Rev Neurosci 2:229.

Vinck M, Oostenveld R, Van Wingerden M, Battaglia F, Pennartz CM (2011) An improved index of phase-synchronization for electrophysiological data in the presence of volume-conduction, noise and sample-size bias. Neuroimage 55:1548–1565.

Viriyopase A, Bojak I, Zeitler M, Gielen S (2012) When Long-Range Zero-Lag Synchronization is Feasible in Cortical Networks. Front Comput Neurosci 6 Available at: https://www.frontiersin.org/articles/10.3389/fncom.2012.00049/full [Accessed January 2, 2020].

Wirsich J, Ridley B, Besson P, Jirsa V, Bénar C, Ranjeva J-P, Guye M (2017) Complementary contributions of concurrent EEG and fMRI connectivity for predicting structural connectivity. NeuroImage 161:251–260.

Womelsdorf T, Schoffelen J-M, Oostenveld R, Singer W, Desimone R, Engel AK, Fries P (2007) Modulation of Neuronal Interactions Through Neuronal Synchronization. Science 316:1609–1612.

Zumer JM, Brookes MJ, Stevenson CM, Francis ST, Morris PG (2010) Relating BOLD fMRI and neural oscillations through convolution and optimal linear weighting. NeuroImage 49:1479–1489.

APPENDIX A: SUPPLEMENTARY MATERIALS

A.1 Analysis of the continuous data

To verify that the large proportion of electrode pairs with uncorrelated time-varying PhC and AmpC (Table. 1) was not driven by the short post-stimulus interval and/or the limited number of time samples of the epoched data, we additionally investigated the continuous data. We extracted time-varying PhC and AmpC from the continuous data without splitting it into epochs. For each electrode pair, we used sliding time windows similar to what was performed on epoched data (c.f. section 2.3 of the main text).

In the absence of epoched trials, we could not measure PhC as the consistency of the phase lags over trials. Instead, we alternatively quantified PhC as consistency of phase lags over several consecutive oscillatory cycles rather than epochs. This alternative measure has been previously shown to be practical in the resting state literature using continuous timecourses (Sadaghiani et al., 2012, 2019):

$$PLV_{continuous}(f) = \sum_{i=1}^{N} e^{j\Delta\varphi_i(f)}$$

Where f is frequency, $\Delta\varphi$ is the difference between instantaneous phases of the two signals, i is the index of time sample, and N is the number of samples within a time window. The sliding window shifting parameter was set to 1s. Following procedures in prior literature (Sadaghiani et al., 2012), the window length was set to 10 seconds, corresponding to 75, 100, 200, 400, and 800 number of oscillatory cycles in the center frequency of theta, alpha, beta, gamma, and high gamma bands, respectively. AmpC was calculated within the same 10s sliding window using the exact same measure of AmpC that we used for the epoched data.

Once time-varying PhC and AmpC were computed, another sliding window was used to assess temporal correlation between PhC and AmpC dynamics across the whole time course. It has been shown that window length in the sliding window approach can have considerable effects on its outcomes (Preti et al., 2017). Thus, in order to find the optimum window length for assessing temporal correlation of PhC and AmpC, we investigated their Power Spectral Density (PSD). For PhC and AmpC, we extracted the PSD of all electrode pairs as shown in Fig. 9. Then, we identified the frequency associated with the peak of each of the PSD curves (narrow vertical black lines). Next, we selected the median of all peaks for PhC and AmpC as representative frequency for that measure (thick vertical dashed lines). Finally, between the two representative frequencies of PhC and AmpC, we selected the smaller one. This choice results in the larger time window (~=58s averaged over subjects and frequency bands) and assures that we can detect at least one cycle of the representative frequency of both measures.

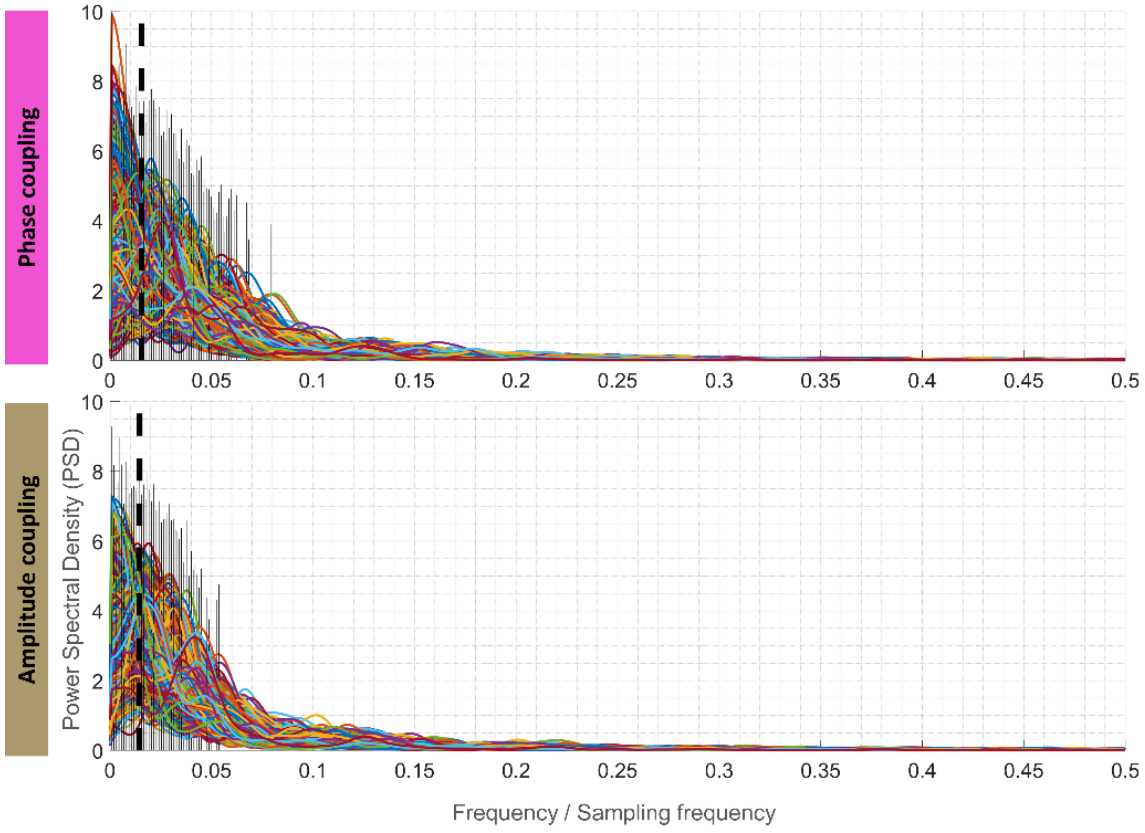

Fig. 9 – Power Spectral Density (PSD) of PhC (top) and AmpC (bottom) across all electrode pairs for a single subject and frequency band shown as an example. Horizontal axis shows frequency divided by the sampling frequency. Note that frequency goes up to 0.5, which is half of the sampling rate of the dynamic assessment of the FC. Narrow black lines show frequencies associated with the peak of the curves, and thick dashed black line shows the median among all the narrow black lines. Between the two dashed black lines, the one closer to zero corresponds to the time window that was used to assess temporal correlation between PhC and AmpC. The optimum time window was estimated individually for each subject and frequency band.

Using the ensuing window length, temporal correlation between PhC and AmpC dynamics was estimated across time and electrode pairs. To test the significance of these correlation values, we used the same null model approach as for the epoched data. Specifically, we generated 500 surrogate data by phase-permuting the PhC and AmpC dynamics and compared the real correlation values with their corresponding null distribution ($q<0.05$; Benjamini-Hochberg FDR-corrected for all electrode pairs and time windows).

Proportion of negatively correlated, uncorrelated, and positively correlated PhC and AmpC dynamics across all electrode pairs and time windows are reported on Table. 2 in the main text. Similar to the results from epoched data (Table. 1), large proportions of the data showed uncorrelated PhC and AmpC temporal dynamics. As an example, histograms of temporal correlation values between PhC and AmpC dynamics of all frequency bands are shown for a single subject in Fig. 10 (bottom row; top row shows corresponding results of epoched data). The zero-centered and largely symmetrical histograms indicate that the two coupling modes are temporally distinguishable, although their spatial organization is highly similar due to the presence of an intrinsic architecture.

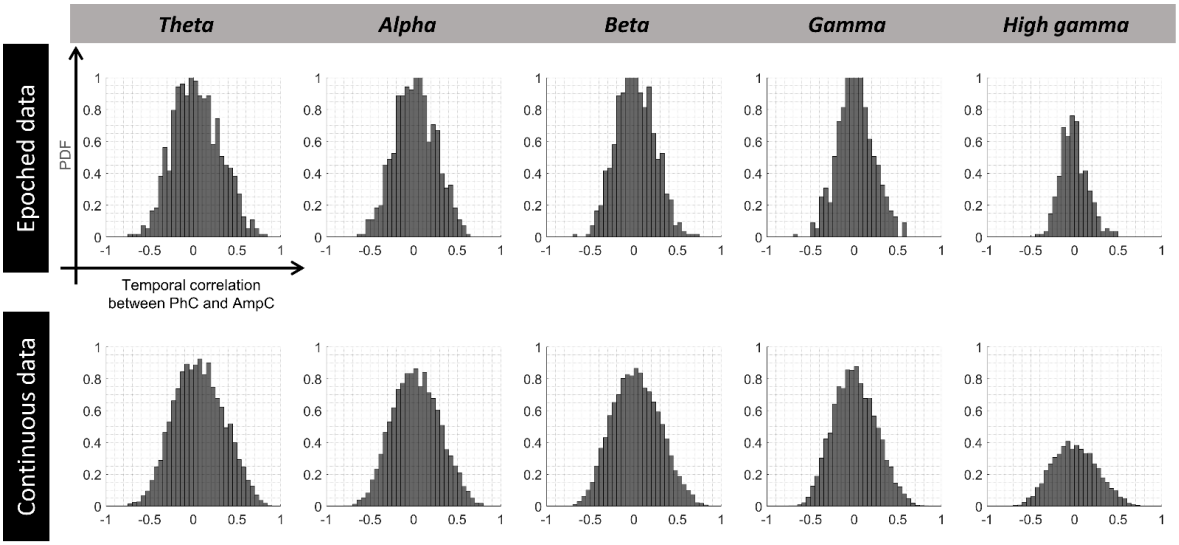

Fig. 10 – Histogram of temporal correlation values between PhC and AmpC time-varying connectivity of a single subject across all electrode pairs. The first row corresponds to the epoched data and the second row to continuous data. Each column shows the histogram of a specific frequency band as labeled. In each subplot, horizontal axis shows the temporal correlation value. Note that the observed discrepancies between histograms of the two rows are due to unavoidable methodological differences (first and foremost window length) used for the epoched and continuous data. Methodological differences notwithstanding, all histograms in both epoched and continuous data are zero-centered and symmetric, indicating the absence of a systematic correlation between time-varying PhC and AmpC.

A.2 Replication with alternative FC measures

Despite minimal volume conductance effects in ECoG surface recordings (Rouse et al., 2016; Dubey and Ray, 2019; Rogers et al., 2019), we wanted to assure that our findings are not largely produced by presence of source leakage in both FC measures. To this end, we remove potential volume conduction effects from one of the FC measures (PhC) to avoid any spurious cross-measure spatial similarities generated by shared artifacts between the measures. We applied weighted phase lag index (wPLI; Vinck et al., 2011) and imaginary part of coherency (ImC; Nolte et al., 2004) as implemented in FieldTrip (http://www.fieldtriptoolbox.org) to estimate PhC. Note that the primary dataset was used for this purpose due to higher number of subjects (N=18).

For both alternative measures, we replicated major findings of results section 3.1 of the main text as shown in Fig. 11. For ImC and wPLI, we confirmed that PhC and AmpC are spatially correlated during the post-stimulus period. Specifically at the group level, spatial correlations exceeded chance level in all frequency bands for both measures (wPLI: $p< 5e\text{-}5$ for *t*-tests in all frequency bands; Similarly for ImC: $p<5e\text{-}4$ in all frequencies). At the single-subject level, the spatial correlation exceeded the individual null model in the majority of 18 (subjects) × 5 (frequency bands) comparisons with few exceptions. For wPLI measure 18, 14, 16, 15, and 16 subjects showed the significant effect from theta to high gamma. Corresponding results for ImC are as follows: 13, 14, 16, 13, and 15 subjects out of 18. The few exceptions and the observed reduction of effect size in comparison to PLV-based results (Fig. 6 & 8A) are likely caused by underestimation of PhC due to suppression of zero-lag connectivity that includes real zero-lagged phase-coupled interactions (see discussion section). Altogether, the observations suggest

that PhC and AmpC are spatially tied to each other during the post-stimulus period irrespective of potential volume conduction.

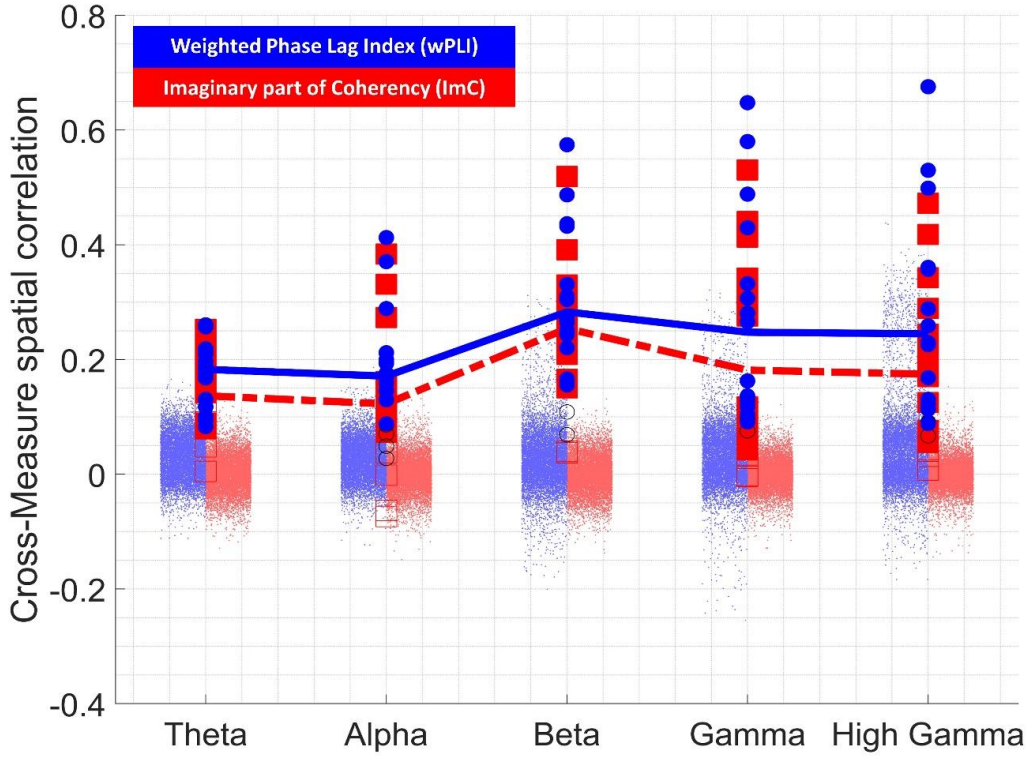

Fig. 11 – Spatial correlation between PhC and AmpC coupling modes during post-stimulus condition using two different measures that suppress zero-lag connections (wPLI and ImC). Y-axis shows spatial correlation and x-axis shows frequency bands as indicated. Blue circles show subjects' individual R values between wPLI and AmpC (filled: significant; unfilled: insignificant). Red squares show corresponding R values between ImC and AmpC. Light blue (or red) dot clouds show surrogate R values derived from wPLI (or ImC), pooled over all subjects. Solid blue line represents grand average R values extracted from wPLI, while dashed red line depicts corresponding result based on ImC measure of PhC. The large number of significant individual R values across all frequencies and the convergence of effects over two different PhC measure that suppressing zero-lag connections suggest that the spatial similarity of PhC and AmpC is not fully explained by volume conduction.

Further, we confirmed findings of results section 3.1.2 of the main text after exclusion of possible volume conduction effects using wPLI and ImC measures. For both measures and all frequency bands (with exception of theta for ImC), we found the reduction of PhC-to-AmpC spatial similarity between post-stimulus compared to task-evoked conditions to be significant

(Benjamini-Hochberg FDR-corrected). For wPLI measure, the group-level *t*-values (and the corresponding p-values) from theta to high gamma were: $t_{theta,17}$= 4.69 (p=1.04e-4), $t_{alpha,17}$= 4.65 (p=1.13e-4), $t_{beta,17}$= 10.34 (p=4.73e-09), $t_{gamma,17}$= 9.10 (p=3.02e-08), $t_{high\ gamma,17}$= 8.99 (p=3.57e-08). Corresponding values for ImC were as follows: $t_{theta,17}$= 1.36 (p=0.096), $t_{alpha,17}$=2.20 (p=0.021), $t_{beta,17}$= 7.97 (p=1.92e-07), $t_{gamma,17}$= 5.52 (p=1.87e-05), $t_{high\ gamma,17}$= 6.08 (p=6.09e-06). This observation supports the conclusion that PhC and AmpC spatial organizations are tied by an intrinsic non-spurious FC that cannot be fully explained by volume conduction.

APPENDIX REFERENCES

Dubey A, Ray S (2019) Cortical Electrocorticogram (ECoG) Is a Local Signal. J Neurosci 39:4299–4311.

Nolte G, Bai O, Wheaton L, Mari Z, Vorbach S, Hallett M (2004) Identifying true brain interaction from EEG data using the imaginary part of coherency. Clin Neurophysiol 115:2292–2307.

Preti MG, Bolton TA, Van De Ville D (2017) The dynamic functional connectome: State-of-the-art and perspectives. NeuroImage 160:41–54.

Rogers N, Hermiz J, Ganji M, Kaestner E, Kılıç K, Hossain L, Thunemann M, Cleary DR, Carter BS, Barba D, Devor A, Halgren E, Dayeh SA, Gilja V (2019) Correlation Structure in Micro-ECoG Recordings is Described by Spatially Coherent Components. PLOS Comput Biol 15:e1006769.

Rouse AG, Williams JJ, Wheeler JJ, Moran DW (2016) Spatial co-adaptation of cortical control columns in a micro-ECoG brain–computer interface. J Neural Eng 13:056018.

Sadaghiani S, Dombert PL, Løvstad M, Funderud I, Meling TR, Endestad T, Knight RT, Solbakk A-K, D'Esposito M (2019) Lesions to the Fronto-Parietal Network Impact Alpha-Band Phase Synchrony and Cognitive Control. Cereb Cortex 29:4143–4153.

Sadaghiani S, Scheeringa R, Lehongre K, Morillon B, Giraud A-L, D'Esposito M, Kleinschmidt A (2012) Alpha-band phase synchrony is related to activity in the fronto-parietal adaptive control network. J Neurosci Off J Soc Neurosci 32:14305–14310.

Vinck M, Oostenveld R, Van Wingerden M, Battaglia F, Pennartz CM (2011) An improved index of phase-synchronization for electrophysiological data in the presence of volume-conduction, noise and sample-size bias. Neuroimage 55:1548–1565.